Quantifying the contributions of atmospheric processes and meteorology to severe PM$_{2.5}$ pollution episodes during the COVID-19 lockdown in the Beijing-Tianjin-Hebei, China

Ishaq Dimeji Sulaymon[a], Yuanxun Zhang[b,c], Philip K. Hopke[d,e], Song Guo[f], Fei Ye[a], Jinjin Sun[a], Yanhong Zhu[a], Jianlin Hu[a*]

[a] *Jiangsu Key Laboratory of Atmospheric Environment Monitoring and Pollution Control, Collaborative Innovation Center of Atmospheric Environment and Equipment Technology, School of Environmental Science and Engineering, Nanjing University of Information Science and Technology, Nanjing, 210044, China*

[b] *College of Resources and Environment, University of Chinese Academy of Sciences, Beijing 100049, China*

[c] *CAS Center for Excellence in Regional Atmospheric Environment, Chinese Academy of Sciences, Xiamen, 361021, China*

[d] *Center for Air Resources Engineering and Science, Clarkson University, Potsdam, NY 13699, USA*

[e] *Department of Public Health Sciences, University of Rochester School of Medicine and Dentistry, Rochester, NY 14642, USA*

[f] *State Key Joint Laboratory of Environmental Simulation and Pollution Control, College of Environmental Sciences and Engineering, Peking University, Beijing, 100871, China*

* Corresponding author. *E-mail address:* sulaymondimeji@nuist.edu.cn; jianlinhu@nuist.edu.cn

Key Points:

- Three severe PM$_{2.5}$ pollution episodes were identified in the Beijing-Tianjin-Hebei region during the COVID-19 lockdown.

- The PM$_{2.5}$ episodes were dominated by emissions and aerosol processes, and enhanced by unfavorable meteorological conditions.

- Designing more effective emissions control strategies with both chemistry and meteorology in thought could mitigate future PM$_{2.5}$ episodes.

Abstract

A major tool for curtailing the spread of COVID-19 pandemic in China was a nationwide lockdown, which led to significant reductions in anthropogenic emissions and fine particulate matter ($PM_{2.5}$). However, the lockdown measures did not prevent high $PM_{2.5}$ pollution episodes (EPs). Three severe EPs were identified in the Beijing-Tianjin-Hebei (BTH) region during the lockdown. The integrated process rate (IPR) analysis tool in the Community Multiscale Air Quality (CMAQ) model was employed to quantify the contributions of individual atmospheric processes to $PM_{2.5}$ formation during the lockdown in the BTH region. The IPR results showed that emissions and aerosol processes were the dominant sources of net surface $PM_{2.5}$ in Beijing and Tianjin, constituting a total of 86.2% and 92.9%, respectively, while emissions, horizontal transport, and aerosol processes dominated the net surface $PM_{2.5}$ in Shijiazhuang and Baoding. In addition, the EPs in Beijing and Tianjin were primarily driven by local emissions, while the EPs in Shijiazhuang and Baoding were attributed to combined local emissions and regional transport. The reductions in $PM_{2.5}$ in Case 2 relative to Case 1 were attributed to the weaker $PM_{2.5}$ formation from emissions and aerosol processes. However, the EPs were enhanced by low planetary boundary layer heights, low vertical export of $PM_{2.5}$ from the boundary layer to the free troposphere, and substantial horizontal import, especially in Shijiazhuang and Baoding. This study improves the understanding of buildup of $PM_{2.5}$ during the EPs, and the results provide insights for designing more effective emissions control strategies to mitigate future $PM_{2.5}$ episodes.

Keywords: Fine particulate matter; Pollution episodes; Process analysis; WRF-CMAQ; COVID-19 shutdown.

1. Introduction

For more than two decades, China has been suffering from severe haze pollution, attributed to its population growth, urbanization, fast industrialization, as well as economic advancement (Li et al., 2020; Shi et al., 2017; Zhao et al., 2021). The development of severe haze is caused by a combination of anthropogenic emissions (local and regional) (Sulaymon et al., 2020, 2021a) and adverse meteorological conditions (Chen et al., 2021; Hua et al., 2021; Hu et al., 2016; Shen, et al., 2021; Shi et al., 2020; Sulaymon et al., 2021a, 2021b). Severe air pollution causes reductions in visibility (Jiang et al., 2021; Li et al., 2019; Wang et al., 2018), changes in climate and ecosystem services (Jiang et al., 2021; Zhao et al., 2021), and adverse human health effects (Chen et al., 2017; Croft et al., 2019; Hopke et al., 2019; Shang et al., 2018; Shen et al., 2020; Yan et al., 2018). The global disease burden (GDB) has attributed about 2 million premature deaths per annum to severe air pollution exposure in China (Yin et al., 2020).

The issuance of the new ambient air quality standards (GB3095-2012) in 2012 and the subsequent implementation of the Air Pollution Prevention and Control Action Plan (APPCAP) in September 2013 by the Chinese authorities has led to reduction in the concentrations of fine particulate matter with aerodynamic diameters of ≤ 2.5 ($PM_{2.5}$) in Chinese cities (Fan et al., 2020; Sulaymon et al., 2021d; Wang et al., 2016). For instance, Xue et al. (2019) noted about 32.5% reduction in the national population-weighed $PM_{2.5}$ annual mean between 2013 and 2017. However, high $PM_{2.5}$ concentrations are still observed in most cities, with annual averages violating the annual Grade I (15 $\mu g/m^3$) and Grade II (35 $\mu g/m^3$) Chinese Ambient Air Quality Standards (CAAQS), and much higher than the WHO (5 $\mu g/m^3$) recommended limit or the USEPA (12 $\mu g/m^3$) standard.

82   The Beijing-Tianjin-Hebei (BTH) region that includes Beijing and Tianjin, and

83   Hebei Province, is one of the most economically developed regions in China. The region

84   has been suffering from severe $PM_{2.5}$ pollution over the past two decades (Chang et al.,

85   2018; Dai et al., 2021a), particularly during the winter season. During past international

86   events (e.g. 2008 Olympic Games, 2014 Asia-Pacific Economic Cooperation, and the 2015

87   Military Parade), Chinese authorities implemented major emissions reductions measures

88   in the BTH region to improve air quality. The effectiveness and success of the emissions

89   reduction policies have been assessed (Wang et al., 2016; Xu et al., 2017; Yang et al., 2016).

90   In December 2019, an outbreak of coronavirus disease (COVID-19) occurred in

91   Wuhan (Zhu et al., 2020) and spread across China and many other countries within a short

92   time. As one of the measures to curtail the spread of COVID-19 pandemic in China, a

93   nationwide lockdown was implemented by the Chinese authorities, leading to significant

94   reductions in anthropogenic emissions and $PM_{2.5}$ concentrations across China (Sulaymon

95   et al., 2021a, 2021c; Wang et al., 2020; Zhao et al., 2020; Zhao et al., 2021). However, the

96   BTH region still experienced high $PM_{2.5}$ pollution episodes during the lockdown

97   (Sulaymon, et al., 2021a; Zhang et al., 2021). Compared to the past international events

98   held in Beijing during the summer and autumn seasons (with no or few pollution episodes),

99   the COVID-19 pandemic occurred in winter, a period with frequent severe pollution events

100   especially in the BTH region. In addition, the COVID-19 lockdown had a longer period

101   with very strict measures than the duration of the past three events.

102   Previous studies have assessed the impacts of COVID-19 lockdown on air quality

103   as well as the relationships between air quality and meteorological conditions during

104   lockdown in BTH region (Cui et al., 2020; Dai et al., 2020; 2021b; Sulaymon et al., 2021a;

4

105 Zhang et al., 2021; Zhao et al., 2021), other regions in China (Gao et al., 2021; Liu et al.,

106 2020; Shen et al., 2021a, 2021b; Sulaymon, et al., 2021c; Wang et al., 2020; Wu et al.,

107 2021; Xing et al., 2020), and outside mainland China (Bashir et al., 2020; Chauhan and

108 Singh, 2020, 2021; Mishra et al., 2021; Muhammad et al., 2020; Orak and Ozdemir, 2021;

109 Querol et al., 2021; Sharma et al., 2020; Singh and Chauhan, 2020; Srivastava, 2021; Ye

110 et al., 2022). A few studies have also been performed on the regional source apportionment

111 of $PM_{2.5}$ during the lockdown (Li et al., 2020; Ma et al., 2021). Li et al. (2020) reported

112 that industry (32.2-61.1%) and residential (2.1-28.5%) were the two highest sources

113 contributing to $PM_{2.5}$ in the Yangtze River Delta (YRD) region, while about 14.0-28.6%

114 contribution was due to long-range transport from northern China. In the BTH region, a

115 few studies have also investigated the source apportionment of $PM_{2.5}$ during lockdown (Cui

116 et al., 2020; Dai et al., 2020). For example, Dai et al. (2020) used Positive Matrix

117 Factorization (PMF) to investigate the sources of $PM_{2.5}$ in Tianjin. Their results showed

118 that secondary inorganic aerosols (SIA) (50.5%), fireworks and residential burning

119 (32.0%), and primary coal combustion emissions (13.3%) were the three dominant sources

120 contributing to $PM_{2.5}$ during the lockdown. Overall, previous studies have reported

121 persistent haze episodes in the BTH region during lockdown despite the emission

122 reductions, and have generally attributed them to unfavorable meteorological conditions

123 (Cui et al., 2020; Dai et al., 2020; 2021b; Sulaymon et al., 2021a; Zhang et al., 2021; Zhao

124 et al., 2021). However, the formation of air pollutants involves various physical processes

125 (such as emissions, condensation, advection, diffusion, deposition, etc.) as well as

126 oxidative chemical process (Huang et al., 2005; Wang et al., 2014; Ye et al., 2022).

127   The process analysis (PA) tool in the Community Multiscale Air Quality (CMAQ)

128   chemical transport model can provide quantitative analysis of the individual contributions

129   of various physical and chemical processes to the observed air pollution (Liu et al., 2010;

130   Liu and Zhang, 2011; Xing et al., 2011; Ye et al., 2022). Liu and Zhang (2011) employed

131   the PA tool to analyze a regional $PM_{2.5}$ pollution episode in the U.S. They found that

132   emissions and aerosol processes such as homogeneous nucleation, heterogeneous

133   nucleation, and condensation were the dominant contributors to increased $PM_{2.5}$

134   concentrations, while horizontal and vertical transport and dry deposition were the primary

135   loss mechanisms. Liu et al. (2010) utilized the PA to explore the contributions of various

136   atmospheric processes on ozone and PM_{10} concentrations in China during four seasons.

137   The results showed that emissions and aerosol processes were the main contributors to

138   PM_{10} concentrations, while horizontal transport was the major removal pathway. Xing et

139   al. (2011) used CMAQ-PA tool to quantify the air quality benefits from emissions

140   reductions and meteorological variations during the 2008 Beijing Olympics. The results

141   indicated that aerosol and emission processes acted as the major $PM_{2.5}$ pathways, while

142   vertical transport was the major $PM_{2.5}$ sink at the surface.

143   Therefore, analyzing the air quality during the unique lockdown period to provide

144   additional understanding of the underlying causes of high pollution episodes even during

145   periods of substantially reduced anthropogenic activity is important for providing

146   approaches to future air quality management strategies. The present study is the first that

147   elucidated the contributions of various atmospheric processes to $PM_{2.5}$ pollution episodes

148   during the lockdown in the BTH region. The results provide new insights into $PM_{2.5}$

149   formation of the three pollution episodes during lockdown. Thus, it provides a valuable

150   example of how to use opportunities like the lockdown period to better understand the

151   causal factors of episodes in other areas of the world, which can then be applied to develop

152   more effective control strategies that would reduce the magnitude of these episodes and

153   better protect public health.

154   **2.**   **Methodology**

155   *2.1.*   *Model set-up and configurations*

156   The Community Multiscale Air Quality model version 5.2 (CMAQv5.2) was

157   applied to simulate the air quality in the BTH region during the COVID-19 lockdown

158   period (January 24-February 29, 2020). The photochemical mechanism and the aerosol

159   module used in configuring the model were the State-wide Air Pollution Research Center

160   version 07 (SAPRC07tic) and AERO6i, respectively (Liu et al., 2020; Sulaymon et al.,

161   2021a, 2021b). Two nested domains with horizontal resolutions of 36 and 12 km were used

162   (Fig. S1). The outer domain (36 km) covers China and the surrounding regions (137 x 107

163   grids), and the inner domain (12 km) covers the study area, the BTH region (127 x 202

164   grids). Each of the two domains had 18 vertical layers, emanating from the surface to a

165   height of about 20 km above the ground level. The initial and boundary conditions (IC/BC)

166   used in the 36 km domain were based on the default profiles provided by the CMAQ model,

167   while the IC/BC used for the 12 km domain were generated from the results of the 36 km

168   simulations. As a way of reducing the impact of initial conditions on $PM_{2.5}$ predictions, the

169   simulations began on January 19, and the results of the first 5 days (January 19-23, 2020)

170   were excluded from the model analysis, thus serving as a spin-up of the model. The

171   meteorological inputs were simulated by the Weather Research and Forecasting (WRF v4.0)

172   model with the FNL reanalysis data serving as the IC/BC. The detailed settings and

173   configurations, including the major physics schemes used in this study are listed in Table

174   S1, while other settings could be found in previous studies where the WRF model was

175   applied (Hu et al., 2015, 2016; Wang et al., 2021).

176   In this study, the Multi-resolution Emission Inventory for China (MEIC) of year

177   2016 (http://www.meicmodel.org) served as the anthropogenic emissions from China. In

178   addition, the anthropogenic emissions from adjacent countries and regions were processed

179   based on the Regional Emission inventory in ASia version 2 (REAS2) (Kurokawa et al.,

180   2013). Biogenic emissions were estimated with the Model of Emissions of Gases and

181   Aerosols from Nature (MEGAN) version 2.1. Open burning emissions were generated

182   based on the data obtained from the Fire INventory from NCAR (FINN) (Wiedinmyer et

183   al., 2011). Sea salt and windblown emissions were generated inline (Sulaymon et al., 2021a,

184   2021b). Further details regarding the emission processing can be found in Hu et al. (2016)

185   and Qiao et al. (2015).

186   To evaluate the impacts of the emissions reductions on air quality, two scenarios

187   (referred to as Cases 1 and 2) were simulated as presented in Table S2. The first scenario

188   (Case 1) used the original MEIC16 emission inventory. In the second scenario (Case 2),

189   emissions from transportation, industry, and power sectors were reduced (Table S2) during

190   the lockdown period, while those of residential and agriculture were similar to Case 1. The

191   basis for adopting the emission reduction factors has been previously presented (Sulaymon

192   et al., 2021a; Wang et al., 2020), and has also been detailed in the Supplementary Material

193   (Text S1). The differences between the results of Cases 1 and 2 represent the impact of

194   emissions reductions on air quality during the lockdown.

195

196 *2.2.   Process analysis*

197   The process analysis (PA) tool embedded in the CMAQ model has been described

198 as a versatile analytical tool for quantifying the contributions of individual atmospheric

199 processes and chemical reactions to a pollutant (Fu et al., 2020; Ye et al., 2022). PA is

200 comprised of two components; the integrated process rate (IPR) and integrated reaction

201 rate (IRR) analysis. The IPR involves the changes in the hourly concentrations of pollutants

202 due to individual atmospheric processes such as gas-phase chemistry, emissions, aerosol

203 processes, dry deposition, cloud processes, and vertical and horizontal transport at each

204 grid cell in the model domain. The IPR analysis has been extensively used in quantifying

205 the contributions individual atmospheric processes to air pollutants (Fan et al., 2015; Fu et

206 al., 2020; Li et al., 2012; Wang et al., 2010; Xing et al., 2011; Ye et al., 2022), hence,

207 detailed information about IPR can be found in these referenced studies.

208   In this study, the IPR module in CMAQv5.2 was employed to resolve both physical

209 and chemical processes involved in the formation of $PM_{2.5}$ during the lockdown period in

210 the BTH region. The IPR results were subsequently used to analyze the individual

211 processes involved in $PM_{2.5}$ formation in the surface layer and full planetary boundary

212 layer (PBL), respectively. For this purpose, the processes considered were the chemistry

213 (gas-phase), emissions, aerosol processes (SOA formation, nucleation, condensation,

214 coagulation, heterogeneous chemistry, mode merging, and aerosol thermodynamics), cloud

215 processes, dry deposition, vertical transport (sum of vertical advection and diffusion), and

216 horizontal transport (sum of horizontal advection and diffusion). Based on their

217 contributions to $PM_{2.5}$ concentrations, atmospheric processes can be grouped into two;

218 source process (concentration increases) and sink process (concentration decreases). Dry

9

219　deposition and emission belong to the sink and source process, respectively. The IPR of

220　other processes can either be source (positive) or sink (negative). The contributions of

221　individual atmospheric processes to the formation of $PM_{2.5}$ were estimated using the

222　approach of Ye et al. (2022):

223 $$\text{SOURCE}_p = \frac{\sum_t \text{IPR}_{p,t}}{\sum_p \sum_t \text{IPR}_{p,t}} \times 100\% \quad (\text{IPR}_{p,t} > 0) \tag{1}$$

224 $$\text{SINK}_p = \frac{\sum_t \text{IPR}_{p,t}}{\sum_p \sum_t \text{IPR}_{p,t}} \times 100\% \quad (\text{IPR}_{p,t} < 0) \tag{2}$$

225　where p is the atmospheric process, and t is the time (in hour). SOURCE_p and SINK_p are

226　the proportions of the atmospheric process p in all source and sink processes, respectively.

227　Both source and sink categories are used to reveal how important an atmospheric process

228　is in influencing the changes in $PM_{2.5}$ concentrations.

229　**3.　Results and discussion**

230　*3.1.　WRF model performance*

231　　　　Meteorological parameters play an important role in the formation and

232　transportation of air pollution (Hu et al., 2016; Sulaymon et al., 2021a, 2021b; Wang et al.,

233　2021). In addition, the influences of meteorological parameters on the air quality

234　simulations using chemical transport model have also been established (Hu et al., 2016;

235　Sulaymon et al., 2021a; Wang et al., 2021). To evaluate the WRF model performance, the

236　predicted temperature (T2) and relative humidity (RH) at 2 m above ground level, and wind

237　speeds (WS) and wind directions (WD) at 10 m above surface were compared to the

238　observational data downloaded from the official website of the Chinese Meteorological

239　Agency (http://data.cma.cn/en, last access: January 2023). Table S3 shows the summary

statistics including the mean observation (OBS), mean prediction (PRE), mean bias (MB), mean error (ME), and the root mean square error (RMSE). In addition to the BTH region as a whole, four representative cities including Beijing (BJ), Tianjin (TJ), Shijiazhuang (SJZ), and Baoding (BD) were evaluated. Generally, T2 (Table S3) was slightly over-predicted in the BTH and the four representative cities during the lockdown. The MB and ME of T2 in BTH were 0.4 and 1.7, respectively, which fell below the suggested benchmarks (MB≤±0.5; and ME≤2.0) (Emery et al., 2001). These are consistent with a previous study over BTH region (Chang et al., 2019). Except in Tianjin (MB:0.5), the MB values in other three cities (Beijing:2.2; Shijiazhuang:0.6; and Baoding:1.3) exceeded the benchmark. Except in Beijing (ME:2.3), the ME values in all the cities were within the benchmark range. Although there were no suggested benchmarks for the MB and ME indices of RH, however, RH (Table S3) was underpredicted in BTH region and the four representative cities (Ma et al., 2021). Similar results had been reported by previous studies over BTH region (Chang et al., 2018; Li et al., 2021b; Sulaymon et al., 2021a; Zhao et al., 2021) and China as a whole (Hu et al., 2016; Sulaymon et al., 2021b; Wang et al., 2021). Bhati and Mohan (2018) obtained a similar result and attributed it to the influence of the boundary layer parameterization on the weather prediction. The mean observed WS across the cities and BTH ranged from 1.8 to 2.3 m/s, an illustration of relatively calm conditions during the lockdown. Generally, WS (Table S3) was over-predicted (Ma et al., 2021). However, based on the ME, MB, and RMSE indices, the predictions reasonably captured the observations across the four cities and BTH (Li et al., 2021b; Sulaymon et al., 2021a; Zhao et al., 2021). The over-predictions of WS might be due to unresolved topography within the WRF model (Li et al., 2014). The MB values met the suggested benchmark

263   (≤±0.5) in BTH and three cities except Shijiazhuang (0.7). During the lockdown, the ME

264   and RMSE values ranged between 0.6-0.9 and 0.7-1.2, respectively, with both indices

265   falling below the recommended benchmarks (≤2.0). WD (Table S3) was generally under-

266   predicted except in Shijiazhuang where the PRE was slightly higher than the OBS. Overall,

267   the MB values were above the suggested criterion range (≤±10) except in Baoding (MB: -

268   0.8), Shijiazhuang (MB:2.3), and BTH (MB: -9.6). Also, the ME values in the four cities

269   and BTH region greatly exceeded the benchmark (≤±30), especially in Shijiazhuang

270   (ME:101.5), Beijing (ME:78.4), and BTH region (ME:70.5). Similar model performance

271   of WD had been reported (Hu et al., 2016; Sulaymon et al., 2021a, 2021b; Wang et al.,

272   2021). Generally, in this study, the WRF model exhibited better performance when

273   compared to previous studies in BTH region (Chang et al., 2019; Li et al., 2021b; Sulaymon

274   et al., 2021a; Zhang et al., 2021; Zhao et al., 2021) and China as a country (Ma et al., 2021;

275   Sulaymon et al., 2021b; Wang et al., 2021). Since the simulated meteorological parameters

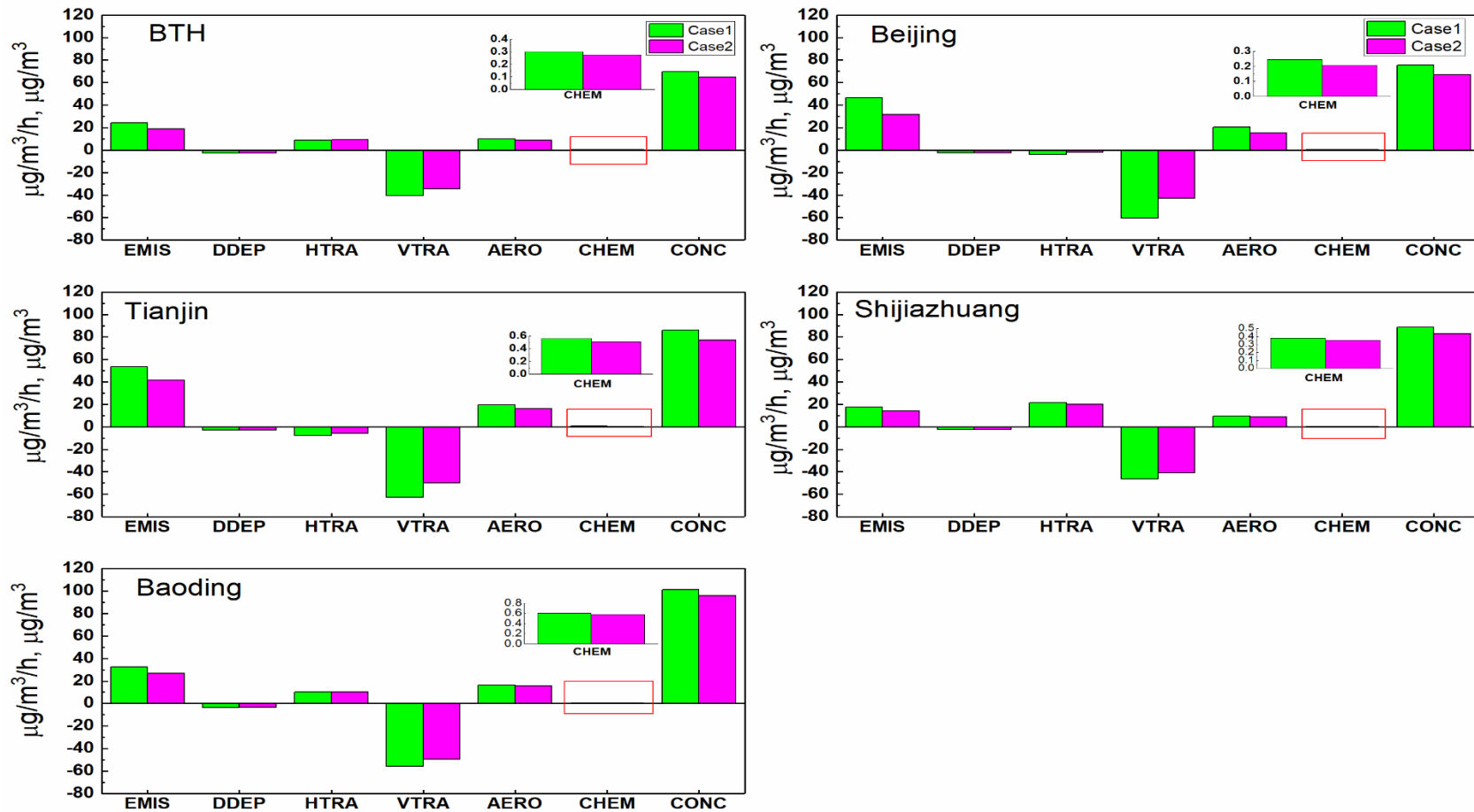276   were robust, they were used in driving the air quality simulations.

277

278   *3.2.   CMAQ model performance*

279   In evaluating the performance of CMAQ model in predicting $PM_{2.5}$, statistical

280   indices, which include the mean observations (OBS), mean predictions (PRE), mean

281   fractional bias (MFB), mean fractional error (MFE), mean normalized bias (MNB), and

282   mean normalized error (MNE) were calculated. The performance of CMAQ model for

283    $PM_{2.5}$ over the BTH and at four representative cities during the lockdown period based on

284   the two cases are shown in Table S4. Generally, the simulated $PM_{2.5}$ concentrations

285   exhibited good agreement with the observed data with the model performance indices

286　falling within the recommended benchmarks for PM$_{2.5}$ (MFB ≤±0.60 and MFE ≤ 0.75)

287　(Boylan and Russel, 2006) in BTH and the four cities for the two cases. For Case 1, PM$_{2.5}$

288　was over-estimated in BTH (0.10), Beijing (0.31), and Tianjin (0.41), while it was under-

289　predicted in Shijiazhuang (-0.05) and Baoding (-0.19). Considering Case 2, all of the MFB

290　values were negative except in Tianjin (0.32), an indication that CMAQ under-predicted

291　the total PM$_{2.5}$ concentrations in BTH and the other three cities. Chang et al. (2019) had

292　reported an under-estimation of PM$_{2.5}$ by CMAQ in Beijing and Shijiazhuang, which is

293　consistent with this study for Case 2. Also, the model performances for Case 2 are in line

294　with the findings of Sulaymon et al. (2021a) In addition, under-predictions of PM$_{2.5}$ in all

295　of the prefectural-level cities of BTH region were reported by Jiang et al. (2021). The MFE

296　values for the two cases ranged between 0.40-0.51, which were within the recommended

297　benchmark (MFE≤ 0.75). Overall, the CMAQ model has shown better performance in this

298　study when compared to previous studies across the BTH region (Chang et al., 2019; Jiang

299　et al., 2021; Li et al., 2021b; Sulaymon et al., 2021a; Zhang et al., 2021; Zhao et al., 2021).

300　Thus, the model results were deemed acceptable for further analyses, including the IPR
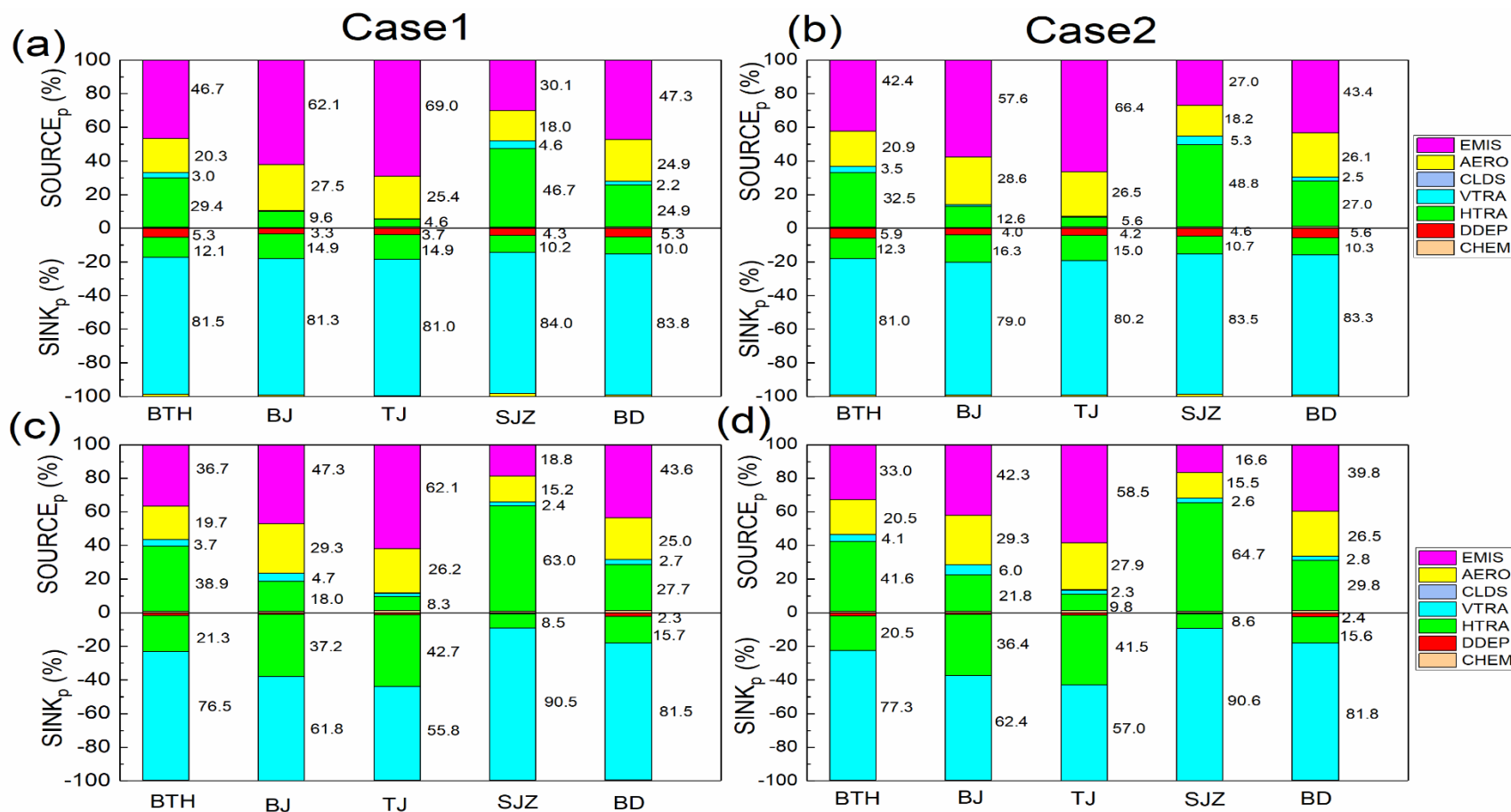
301　analysis.

302　*3.3.　IPR analysis of PM$_{2.5}$ formation at the surface layer*

303　　　　The hourly concentrations of PM$_{2.5}$ as well as the contributions of the individual

304　atmospheric processes to the evolution of PM$_{2.5}$ at the surface layer in the BTH region and

305　four representative cities for the two cases during the lockdown period are illustrated in

306　Fig. 1. In the BTH region as a whole, the emissions (EMIS), horizontal transport (HTRA),

307　and aerosol processes (AERO) were the major positive contributors (sources) to the net

308　surface PM$_{2.5}$.

Fig. 1. Contributions of the individual processes to the concentrations of PM$_{2.5}$ at the surface layer in Cases 1 and 2 during the lockdown period. EMIS represents PM$_{2.5}$ input by emissions, DDEP represents PM$_{2.5}$ decrease by dry deposition; HTRA and VTRA represent PM$_{2.5}$ change by horizontal and vertical transport, respectively; AERO represents PM$_{2.5}$ change by the aerosol; and CHEM represents PM$_{2.5}$ change by gas-phase chemistry. The unit of the processes is μg/m^3/h. CONC is the hourly PM$_{2.5}$ concentrations in μg/m^3.

14

314   For Case 2, the contributions of EMIS, HTRA, and AERO to $PM_{2.5}$ formation were 42.4,

315   32.5, and 20.9% (Fig. 2b), respectively, while their contributions in the same order for Case

316   1 were 46.7, 29.4, and 20.3% (Fig. 2a), respectively. The reduction in the surface layer's

317   $PM_{2.5}$ for the two cases was primarily attributed to the vertical transport (VTRA), while

318   slight removal was also due to dry deposition (DDEP). In Beijing and Tianjin, EMIS and

319   AERO were the predominant processes that contributed to the net surface $PM_{2.5}$ formation

320   (Fig. 1) for both cases. The total contribution ratios of EMIS and AERO in Case 2 were

321   86.2% and 92.9% for Beijing and Tianjin (Fig. 2b), respectively. The reduction of surface

322   $PM_{2.5}$ in Beijing and Tianjin for the two cases was associated with the VTRA, HTRA, and

323   DDEP processes, with VTRA being the highest sink, with negative contributions of 79.0-

324   81.3% (Beijing) and 80.2-81.0% (Tianjin). The results of the present study are consistent

325   with those reported by Ye et al. (2022) in the coastal city of Kannur, India, where the EMIS,

326   HTRA, and AERO were the dominant processes that positively contributed to $PM_{2.5}$

327   evolution, while VTRA and DDEP were responsible for surface $PM_{2.5}$ removal during the

328   three periods considered in the study. Also, Fan et al. (2015) reported EMIS and VTRA as

329   the two major processes that influenced $PM_{2.5}$ at the surface layer in the Pearl River Delta

330   (PRD) region of China. Furthermore, Liu et al. (2010) and Xing et al. (2011) had earlier

331   reported EMIS and AERO as the major $PM_{2.5}$ sources in both surface layer and the PBL in

332   Beijing, while Xing et al. (2011) found VTRA as the major $PM_{2.5}$ sink in the surface layer.

333   The $PM_{2.5}$ removal due to HTRA and DDEP in both cases were relatively the same in both

334   Beijing and Tianjin. Considering Shijiazhuang and Baoding, similar trends were obtained

335   regarding the contributions of individual processes to $PM_{2.5}$ formation.

336
337

15

Fig. 2. Positive and negative contribution ratios of the individual processes to PM$_{2.5}$ concentrations (a,b) at the surface layer and (c,d) in the planetary boundary layer in Cases 1 and 2 during the lockdown period. EMIS, AERO, CLDS, VTRA, HTRA, DDEP, and CHEM represent the contributions of the emissions, aerosol, clouds, vertical transport, horizontal transport, dry deposition, and gas-phase chemistry, respectively to PM$_{2.5}$ formation.

343   The EMIS, AERO, and HTRA processes dominated the positive contributions to

344   the net surface $PM_{2.5}$ in the two cities (Fig. 1), accounting for a total of 94.0 and 96.5% in

345   Shijiazhuang and Baoding, respectively in Case 2 (Fig. 2b), while similar contributions

346   were obtained in Case 1 (Fig. 2a). In addition to EMIS and AERO processes, the horizontal

347   import of $PM_{2.5}$ to the surface layer via HTRA contributed to the elevated $PM_{2.5}$

348   concentrations in both Shijiazhuang and Baoding relative to Beijing and Tianjin. VTRA

349   dominated the removal of $PM_{2.5}$ from the surface layer to upper layers in both cities, with

350   higher rates in Case 1 relative to Case 2. DDEP process also had negative effects on $PM_{2.5}$

351   formation in the two cities, with very low contributions, especially in Shijiazhuang. The

352   photochemistry (CHEM) process had positive net impacts on $PM_{2.5}$ evolution for the two

353   cases across the BTH region and the four representative cities, however, the contributions

354   were extremely low and negligible (Fan et al., 2015). This is contrary to what was reported

355   in Kannur (Ye et al., 2022), as CHEM had negative effects on $PM_{2.5}$ in the city. Due to the

356   negligible contributions of cloud (CLDS) processes to $PM_{2.5}$, it was not discussed in this

357   study. It should be noted that the $PM_{2.5}$ concentrations in BTH region and the four cities in

358   Case 2 were relatively low compared to Case 1. This could be attributed to low $PM_{2.5}$

359   formation from EMIS in Case 2. However, there was no substantive decrease in $PM_{2.5}$

360   concentrations in Case 2 despite reductions in anthropogenic emissions. This could be

361   explained by the reduced $PM_{2.5}$ export from the surface layer to the upper layers due to low

362   VTRA rates in Case 2 (compared to Case 1), leading to the accumulation of $PM_{2.5}$ in the

363   surface layer, which subsequently led to high $PM_{2.5}$ pollution during the lockdown period.

364

365

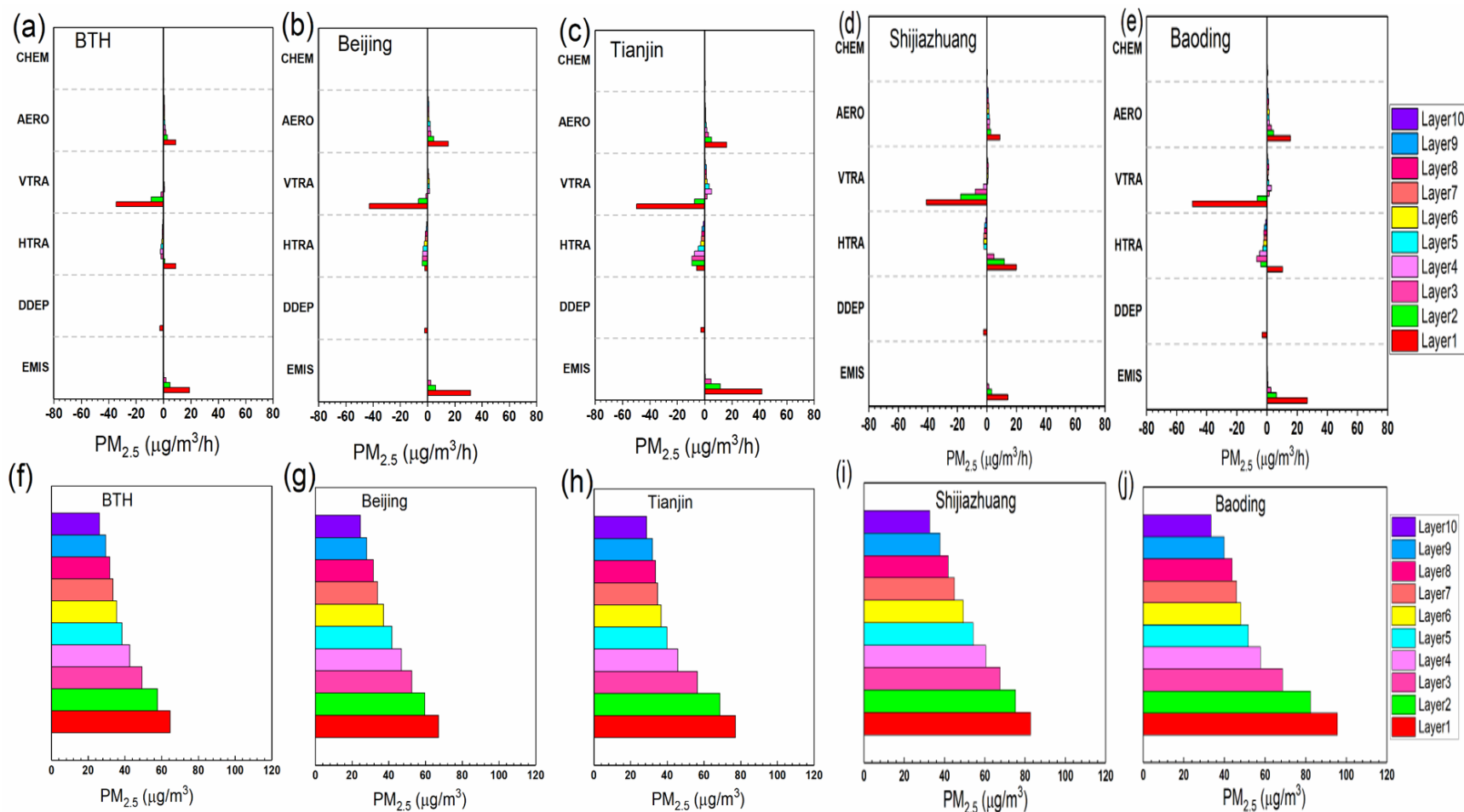*3.4.*   *IPR analysis of PM$_{2.5}$ formation in the PBL*

Fig. S2 shows the mean hourly change rates attributed to individual atmospheric processes to PM$_{2.5}$ production and the concentrations of PM$_{2.5}$ in the PBL during the lockdown. The contributions of the various processes to PM$_{2.5}$ formation within the PBL in BTH and the four cities followed the similar trends as found in the surface layer. However, the contributions of the individual processes to PM$_{2.5}$ were smaller in the PBL compared to the surface layer, as PM$_{2.5}$ concentrations decrease as vertical layers increase (Fan et al., 2015). Generally, the contributions of EMIS and VTRA to the net PM$_{2.5}$ (Case 2) were low in the PBL compared to the surface layer. For instance, relative to what was obtained to the surface layer, the rates due to EMIS and VTRA in the PBL decreased by half in BTH region and all of the representative cities. Similar to the surface layer, the EMIS, HTRA, and AERO were the predominant contributors to the net PM$_{2.5}$ in the whole BTH region and Baoding, while only EMIS and AERO processes contributed substantially to the net PM$_{2.5}$ in Beijing and Tianjin. In Shijiazhuang, however, HTRA was the dominant contributor to PM$_{2.5}$ formation. Compared to other processes, the contributions of CHEM process were extremely low and negligible (Fan et al., 2015; Ye et al., 2022). In addition to VTRA as the major process responsible for the removal of PM$_{2.5}$ across the study areas, PM$_{2.5}$ removal in Beijing and Tianjin was also associated with HTRA. In all of the study areas, slight removal of PM$_{2.5}$ was also attributed to DDEP process. It could be noted that the VTRA and HTRA effects within the PBL were opposite to those to the surface layer. As illustrated in Fig. 2(d), the negative contributions (sinks) due to VTRA in the entire PBL substantially reduced in all of the study areas except Shijiazhuang (increased) when compared to the surface layer. Contrary to the surface layer, the sinks (PM$_{2.5}$ removal) due

18

389   to HTRA within the PBL increased in all of the study areas except Shijiazhuang

390   (decreased). It is worth noting that despite the decreases in EMIS rates by half (which might

391   have adversely influenced $PM_{2.5}$ formation within the PBL) in comparison to the surface

392   layer, the absolute difference in $PM_{2.5}$ concentrations between the surface layer and PBL

393   was not significant, and ranged between 5.7-9.1 $\mu g/m^3$ across the study areas. This could

394   be attributed to reduced $PM_{2.5}$ export due to low VTRA rates, leading to the accumulation

395   of $PM_{2.5}$ within the PBL, and subsequently resulted to high $PM_{2.5}$ concentrations. Overall,

396   in the PBL, EMIS and VTRA served as the two dominant processes that impacted $PM_{2.5}$

397   in BTH, Beijing, Tianjin, and Baoding, while VTRA and HTRA were the two major

398   processes that influenced $PM_{2.5}$ formation in Shijiazhuang.

399   *3.5.   Vertical profiles of the atmospheric processes contributing to $PM_{2.5}$*

400   The mean hourly $PM_{2.5}$ change rates attributed to individual atmospheric processes

401   for the first ten layers (layers 1-10), as well as the vertical profiles of $PM_{2.5}$ evolution for

402   Case 2 during the lockdown period are illustrated in Fig. 3, while that of Case 1 are shown

403   in Fig. S3. As earlier stated in section 3.4, the characteristics of $PM_{2.5}$ concentrations at

404   upper layers (layer 4 and above) were different from near-surface layers, hence, the

405   contributions of emissions sources at upper layers were negligible (Fan et al., 2015). Across

406   the study areas, the contributions from EMIS sources were only found within layers 1-3

407   (Fig. 3a-e) (Fan et al., 2015; Ye et al., 2022), and this was associated with the height of the

408   emissions sources (Fan et al., 2015; Ye et al., 2022). The highest and lowest contributions

409   of EMIS were found in Tianjin and Shijiazhuang, respectively, and the contribution

410   decreased as the vertical layer increased. Within the first three layers, AERO process was

411   another major source of $PM_{2.5}$ in all of the study areas, and the formation rate of $PM_{2.5}$

19

412 through the AERO process decreased as the vertical layer increased. Furthermore, VTRA

413 contributed negatively and served as the predominant sink for removing the near-surface

414 $PM_{2.5}$ at the lower layers in Beijing (layers 1-3), Shijiazhuang (layers 1-4), Tianjin and

415 Baoding (layers 1-2), while it slightly contributed positively (acted as source) at the upper

416 layers. This is consistent with the results of Fan et al. (2015), in which VTRA was reported

417 as a sink in the near-surface layers and a source in the upper layers (layer 4 and above). In

418 Beijing (Fig. 3b) and Tianjin (Fig. 3c), HTRA served as another sink for $PM_{2.5}$ across the

419 vertical layers, and the rate initially increased between layers 1 and 2, but continuously

420 decreased as the vertical layer increased. In Shijiazhuang (Fig. 3d), HTRA contributed

421 positively at the lower layers (layers 1-3) and negatively at the upper layers. Considering

422 Baoding (Fig. 3e), HTRA only acted as the source at the first layer, while it behaved as the

423 sink from the second layer upward. It could be deduced that there were vertical and

424 horizontal exports of $PM_{2.5}$ in Beijing and Tianjin at the surface layer, while Shijiazhuang,

425 Baoding, and the whole BTH region witnessed vertical export and horizontal import of

426 $PM_{2.5}$ in the surface layer. DDEP acted as another sink of $PM_{2.5}$, and only existed at the

427 first layer across the study areas (Fan et al., 2015; Ye et al., 2022). DDEP contributions

428 were only found in the first layer because dry deposition was treated as a bivariate variable

429 by the CMAQ model, and integrated it over the whole atmospheric column (Fan et al.,

430 2015). As shown in Fig. 3(f-j), the highest $PM_{2.5}$ concentration was found in the surface

431 layer, and decreased with increases in vertical layer height (Fan et al., 2015). This result

432 could be attributed to the contributions of EMIS and AERO processes, as well as the

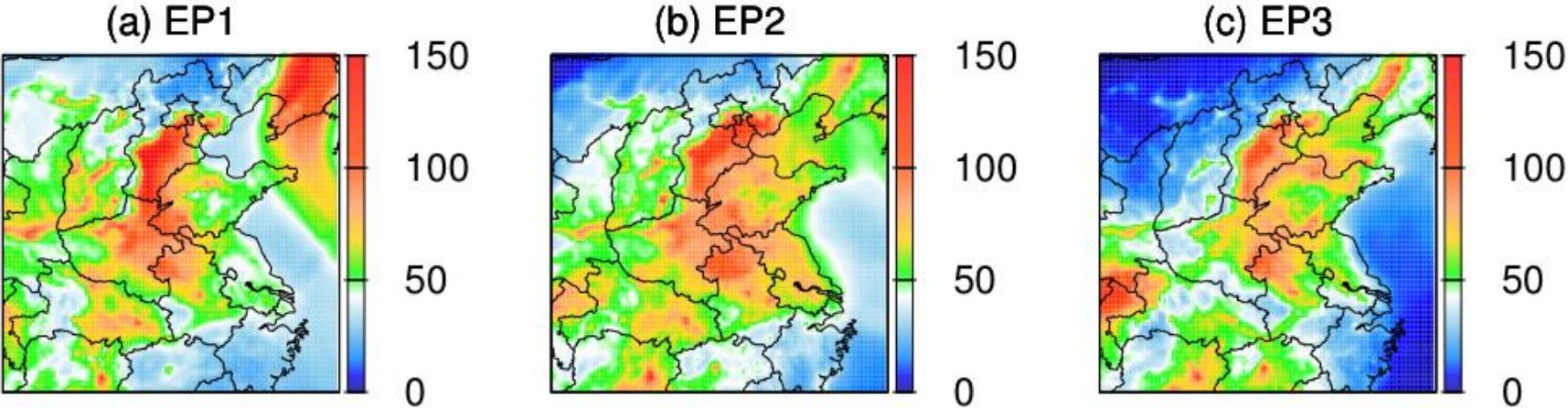433 decreasing trends of the two processes as the vertical layer increased.

434

Fig. 3. Hourly PM$_{2.5}$ change rates due to individual atmospheric processes for layers 1-10 (a-e) and evolution of hourly PM$_{2.5}$ vertical profiles (f-j) in Case 2 during the lockdown period. Abbreviations used in this figure are the same as in Fig. 1.

439 *3.6   IPR analysis of PM$_{2.5}$ pollution episodes during lockdown*

440   During the lockdown period, the predicted PM$_{2.5}$ concentrations (in Case 2) (Fig.4;

441 Tables S5-S6) indicated that persistent PM$_{2.5}$ pollution episodes could not be avoided in

442 the BTH region despite reductions in anthropogenic emissions (Sulaymon et al., 2021a).

443 Fig. S6 illustrates the spatial distributions of PM$_{2.5}$ in the BTH region during the lockdown

444 for the two cases. Fig. S6(b) shows that the PM$_{2.5}$ concentrations during the lockdown were

445 higher (PM$_{2.5}$≥75 µg/m^3, level II of Chinese air quality standard) in Tianjin and southern

446 Hebei Province, while the northern Hebei was characterized with low concentrations

447 (PM$_{2.5}$≤50 µg/m^3). In the prefectural-level cities of BTH region, three severe PM$_{2.5}$

448 pollution episodes (EPs) (Fig. 4) occurred during the lockdown (Case 2). They are

449 represented as EP1 (January 24-31, 2020), EP2 (February 7-13), and EP3 (February 19-

450 21). It should be noted that EP1 and EP2 coincided with the 2020 Spring (January 25) and

451 Lantern (February 8) festivals, respectively. The statistics for all the EPs in each city are

452 enumerated in Tables S5-S6. For the purpose of process analysis of PM$_{2.5}$ during the EPs,

453 Beijing, Tianjin, Shijiazhuang, and Baoding were selected as the representative cities. As

454 illustrated in Fig. 5, Beijing and Tianjin had the highest PM$_{2.5}$ concentrations during EP2,

455 while Shijiazhuang and Baoding recorded their highest PM$_{2.5}$ concentrations during EP1.

456 Also, during EP2 and EP3, Baoding experienced severe pollution with elevated PM$_{2.5}$

457 concentrations. This indicates that the region suffered severe pollution episodes during the

458 lockdown. Dai et al. (2021) and Sulaymon et al. (2021a) had previously reported severe

459 haze episodes in the BTH region during the lockdown. Therefore, it becomes pertinent to

460 elucidate the major atmospheric processes responsible for the formation of the EPs.

461

462

463

Fig. 4. Spatial distributions of predicted PM$_{2.5}$ (Case 2) during (a) EP1, (b) EP2, and (c) EP3 in the BTH region. Units are μg/m^3.
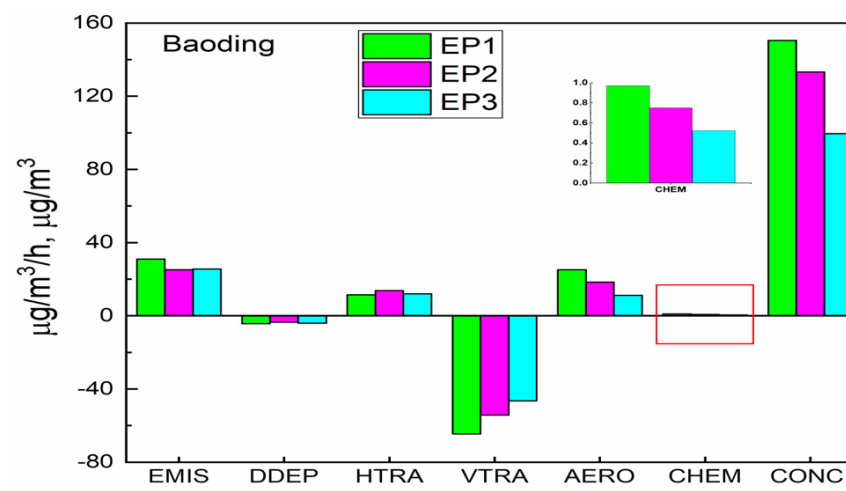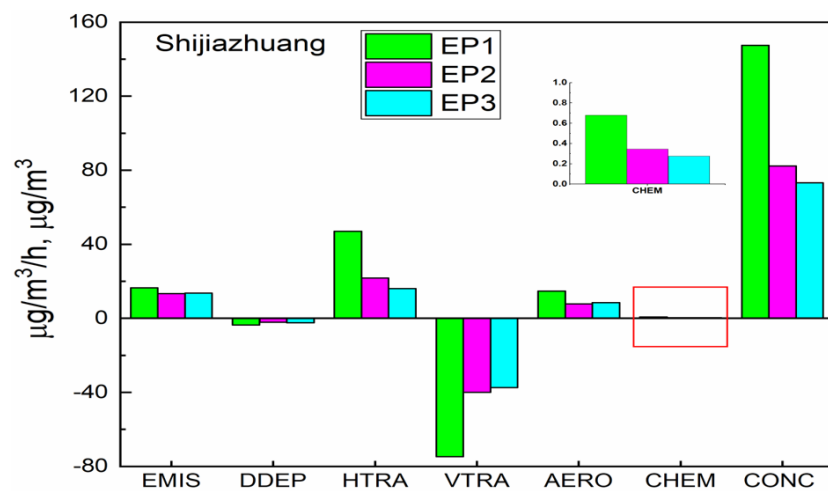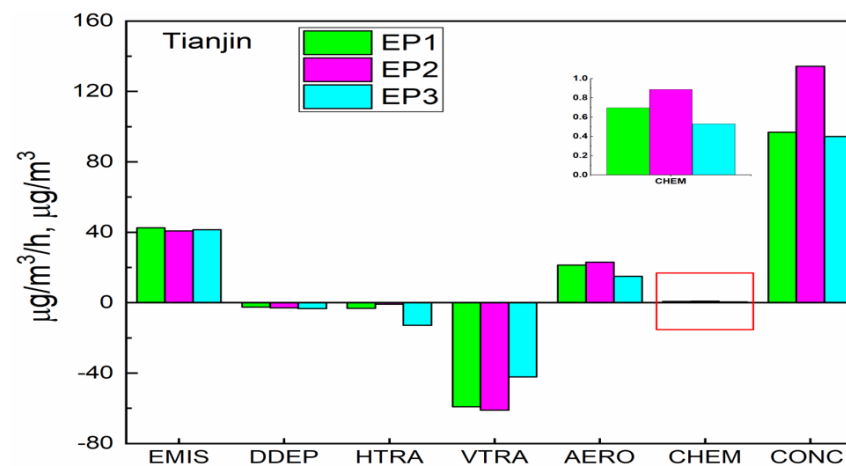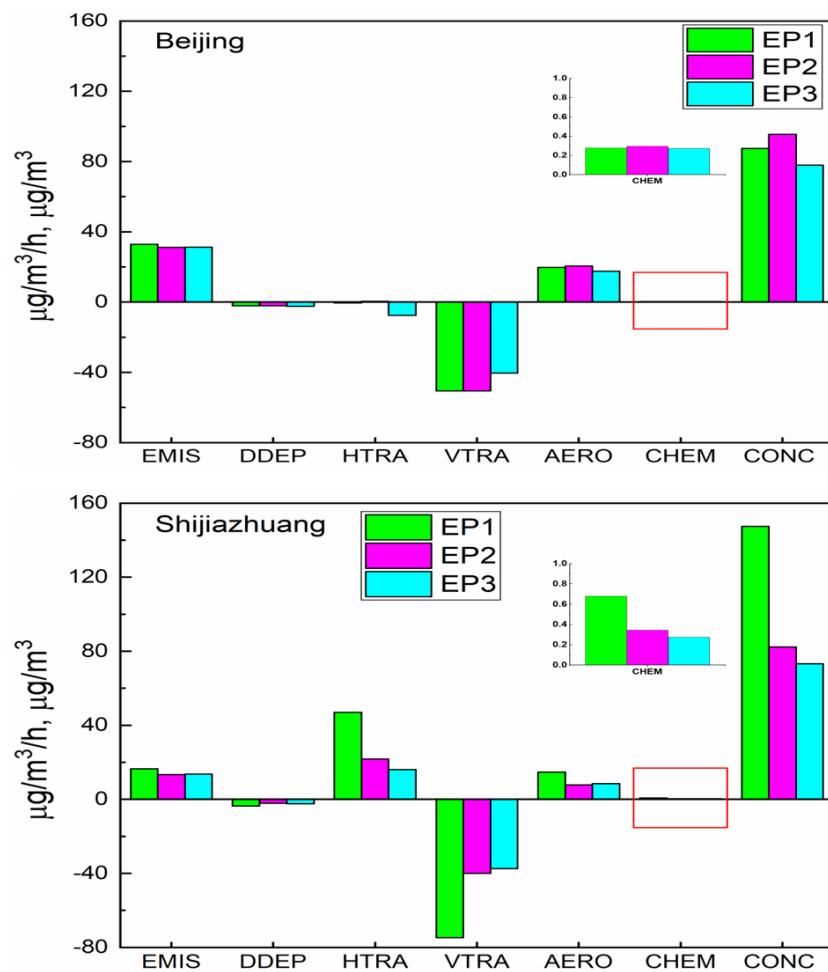
465

466

467

468

469

470

471

472

473

474

Fig. 5. Contributions of the individual processes to the concentrations of $PM_{2.5}$ (Case 2) at the surface layer during the three pollution episodes in the four representative cities. Abbreviations used in this figure are the same as in Fig. 1.

479   The contributions of different atmospheric processes to PM$_{2.5}$ formation (in Case 2) during

480   the three EPs in the four representative cities were analyzed. Table S7 shows the average

481   planetary boundary layer height (PBLH) and wind speed for the four cities during the three

482   EPs. The PBLH during the third pollution episode (EP3; PBLH>400 m) was higher than

483   the PBLH during the first two pollution episodes (EP1 and EP2; PBLH<370 m) across the

484   study areas. A thinner boundary layer is more conducive for the accumulation of locally-

485   emitted particles, leading to increased PM$_{2.5}$ concentrations and results in haze events (Fan

486   et al., 2015). As illustrated in Fig. 5, the three pollution episodes in Beijing and Tianjin

487   were principally caused by local emissions (EMIS), while the pollution events in

488   Shijiazhuang and Baoding could be attributed to both local emissions (EMIS) and regional

489   transport (HTRA).

490   Fig. 5 shows that emissions sources and aerosols were the major positive

491   contributors to PM$_{2.5}$ pollution in Beijing, Tianjin, and Baoding, while horizontal transport

492   was the most significant positive contributor to pollution level in Shijiazhuang, followed

493   by emissions and aerosols. In Baoding, however, HTRA also contributed positively

494   towards PM$_{2.5}$ concentrations throughout the three episodes. There were no significant

495   differences between emissions sources among the three episodes in all of the study areas,

496   and the average total emissions ranged between 13.3-42.6 μg/m^3/h across the EPs in the

497   cities. During the three episodes across the four cities, PM$_{2.5}$ was released into the

498   atmosphere through EMIS and AERO processes, and fell back to the surface layer via

499   DDEP process (Fan et al., 2015), with very low rates of dry deposition (ranged between -

500   2.1 μg/m^3/h and -4.3 μg/m^3/h). Also, PM$_{2.5}$ was transported and diffused through VTRA

501   and HTRA processes. In Beijing and Tianjin, there were negligible differences between
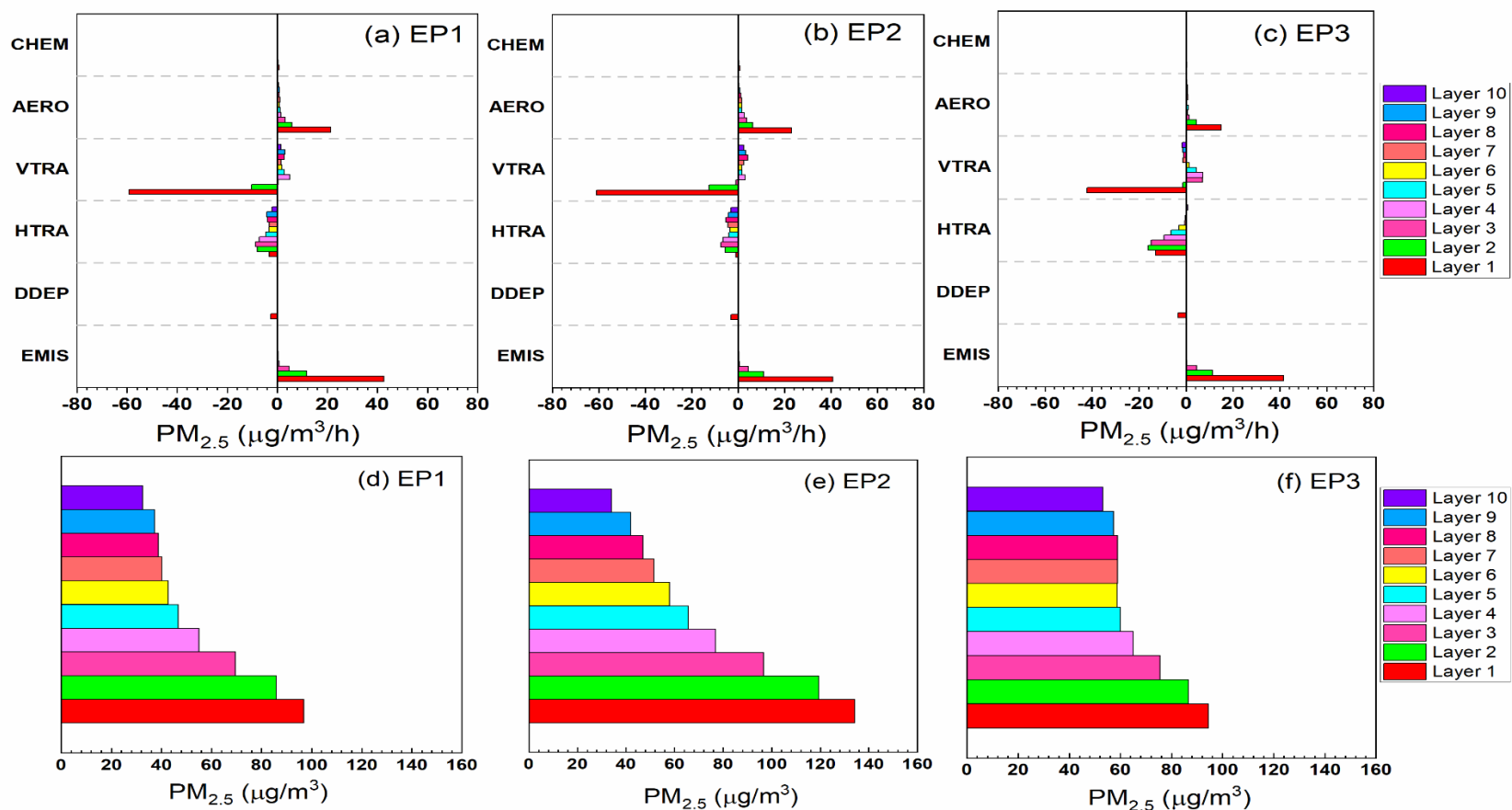
25

502   the contributions from VTRA during the first two episodes, and the total rates were

503   approximately -51 μg/m³/h and -60 μg/m³/h in Beijing and Tianjin, respectively. During

504   EP3 in the two cities, the contributions by VTRA (-40 μg/m³/h in Beijing; and -42 μg/m³/h

505   in Tianjin) were low relative to the first two episodes. The VTRA contributions in

506   Shijiazhuang (-75 μg/m³/h) and Baoding (-65 μg/m³/h) during EP1 were greater than those

507   contributed in Beijing and Tianjin during the same period, and this was due to lower PBLH

508   values (Table S7) in Shijiazhuang and Baoding relative to Beijing and Tianjin. The

509   difference in the VTRA rates between the first two episodes and the third episode in Beijing

510   and Tianjin could be explained by the accumulation of particulates on near-surface layers

511   due to the nature of boundary layer (thinner) (Fan et al., 2015) being exhibited during the

512   first two pollution episodes. Therefore, VTRA had a greater clearing impact for $PM_{2.5}$

513   during the first two episodes in the two cities. Contrarily, during the third episode in the

514   two cities, a more uniform vertical mixing of $PM_{2.5}$ was achieved, and this was due to the

515   thicker PBLHs during EP3 (Table S7). Hence, the clearing effect of VTRA during EP3

516   was low compared to EP1 and EP2. In addition, due to higher wind speed during EP3

517   (Table S7), the negative contributions due to HTRA were higher in Beijing (-8 μg/m³/h)

518   and Tianjin (-13 μg/m³/h) during EP3 compared to EP1 and EP2, and this subsequently

519   reduced the contributions from VTRA during EP3. In Shijiazhuang, VTRA also exhibited

520   a very greater clearing effect during EP1 than EP2 and EP3, and similar scenario also

521   occurred in Baoding. In Shijiazhuang, HTRA was the dominant positive contributor to

522    $PM_{2.5}$ throughout the episodes, with the highest contribution rate during EP1. In Baoding,

523   however, there was negligible difference between the contributions from HTRA to $PM_{2.5}$

524   pollution during the three episodes. Due to availability of several emissions sources in

26

525 Beijing and Tianjin, which result to a large quantity of local emissions, $PM_{2.5}$

526 concentrations were generally higher in the two cities. Hence, the effects of both VTRA

527 and HTRA on pollution levels were negative during the three pollution episodes, and both

528 mainly provided dilution and clearing effects in the two cities (Fan et al., 2015). On the

529 other hand, in both Shijiazhuang and Baoding, horizontal transport contributed positively

530 and significantly increased $PM_{2.5}$ concentrations during the three episodes. It is also worthy

531 to mention that $PM_{2.5}$ concentrations during the three episodes in the four cities were

532 greatly and positively influenced by the planetary boundary layer height, as the episode

533 with the lowest PBLH had the highest $PM_{2.5}$ concentration in a city. The results of the

534 present study are consistent with those reported by Fan et al. (2015) during three pollution

535 episodes over the PRD region. Fan et al. (2015) had reported surface emissions, aerosol

536 processes, and horizontal transport as the major contributors to air pollution episodes over

537 the PRD. In the PBL (Fig. S7), EMIS and AERO were also the dominant contributors to

538 $PM_{2.5}$ concentrations in Beijing and Tianjin, HTRA was the most important source in

539 Shijiazhuang, and EMIS, AERO, and HTRA actively contributed to $PM_{2.5}$ formation in

540 Baoding during the EPs. VTRA was the major removal pathway. However, the

541 contribution and removal rates were low in the PBL relative to the surface layer.
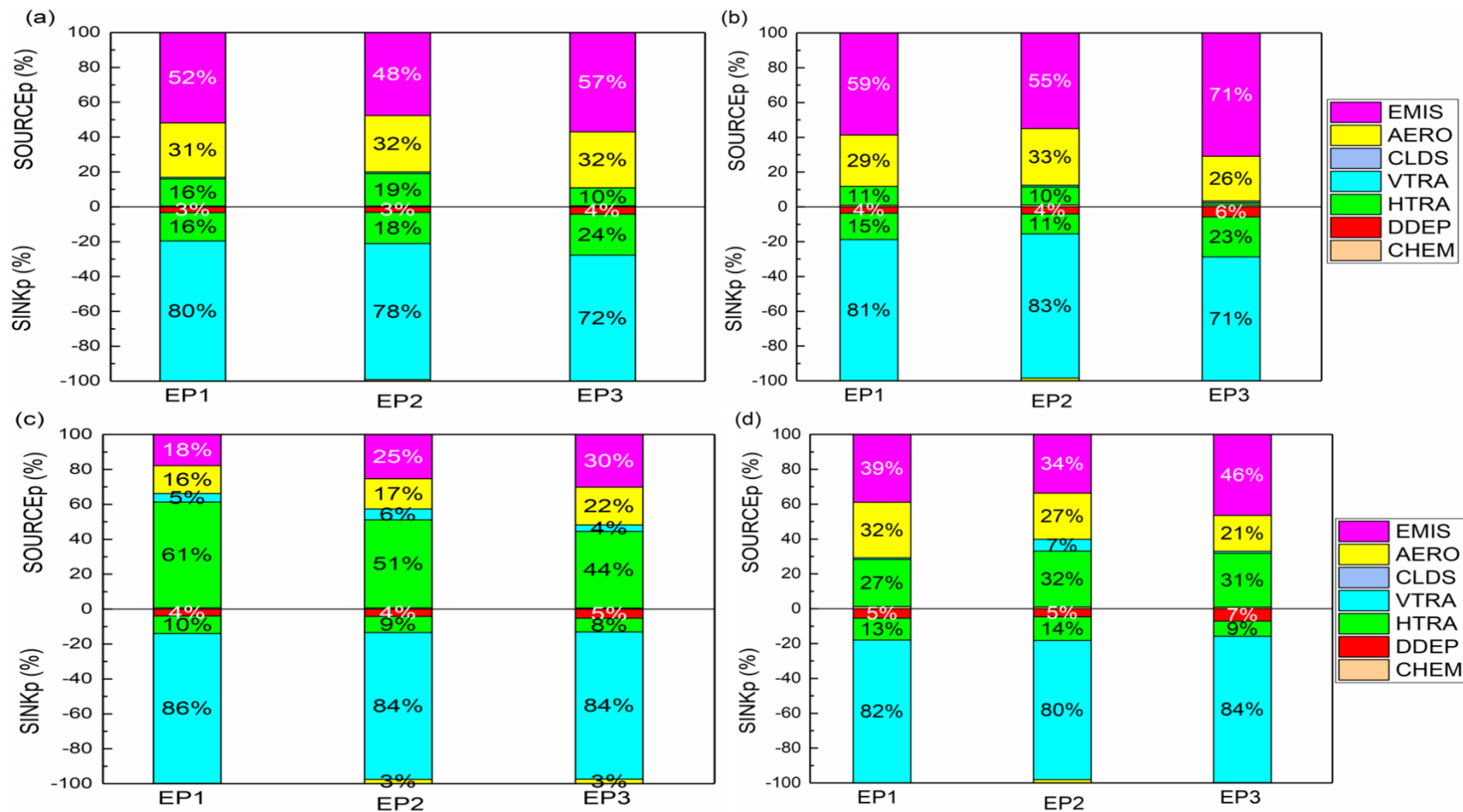
542   To better understand the roles of the atmospheric processes towards the pollution

543 episodes, $PM_{2.5}$ formation and removal within the PBL (layers 1-10) were analyzed in

544 Tianjin (Fig. 6), while those of other three cities are illustrated in Figs S8-S10. Considering

545 the three EPs in Tianjin, the positive contributions of EMIS and AERO processes to the

546 hourly $PM_{2.5}$ significantly occurred within layers 1-3 (Fig. 6a-c), while they both

547 contributed less at upper layers. Also, there were vertical imports of $PM_{2.5}$ (although very

548   low) at upper layers (layers 3-10 for EP1 and EP2; and layers 3-6 for EP3). Conversely,

549   VTRA (layers 1-2) and HTRA (layers 1-10) served as the predominant sinks and $PM_{2.5}$

550   removal pathways. DDEP process also acted as another sink for $PM_{2.5}$ during the EPs, and

551   only existed at the first layer (Fan et al., 2015). The contributions by CHEM process were

552   negligible across the vertical layers (Fan et al., 2015; Ye et al., 2022). As shown in Fig.

553   6(d-f), EP2 was characterized with the highest $PM_{2.5}$ concentrations, followed by EP1 and

554   EP3. Furthermore, the $PM_{2.5}$ formation processes in the surface layer during the EPs were

555   compared. Fig. 7 illustrates the percentage contributions of the atmospheric processes to

556   $PM_{2.5}$ formation/removal during the EPs in the four cities. The total contributions of EMIS

557   and AERO (EMIS+AERO) during the EPs ranged between 80-89% and 88-97% in Beijing

558   (Fig. 7a) and Tianjin (Fig. 7b), respectively. In Shijiazhuang (Fig. 7c), the contributions

559   due to HTRA during the episodes ranged between 44-61%, making it the major $PM_{2.5}$

560   source. As earlier revealed in Fig. 5, $PM_{2.5}$ formation during the episodes in Baoding (Fig.

561   7d) was attributed to the contributions of EMIS, AERO, and HTRA, with total

562   contributions of 93-98% during the EPs. In the four cities, $PM_{2.5}$ removal was dominantly
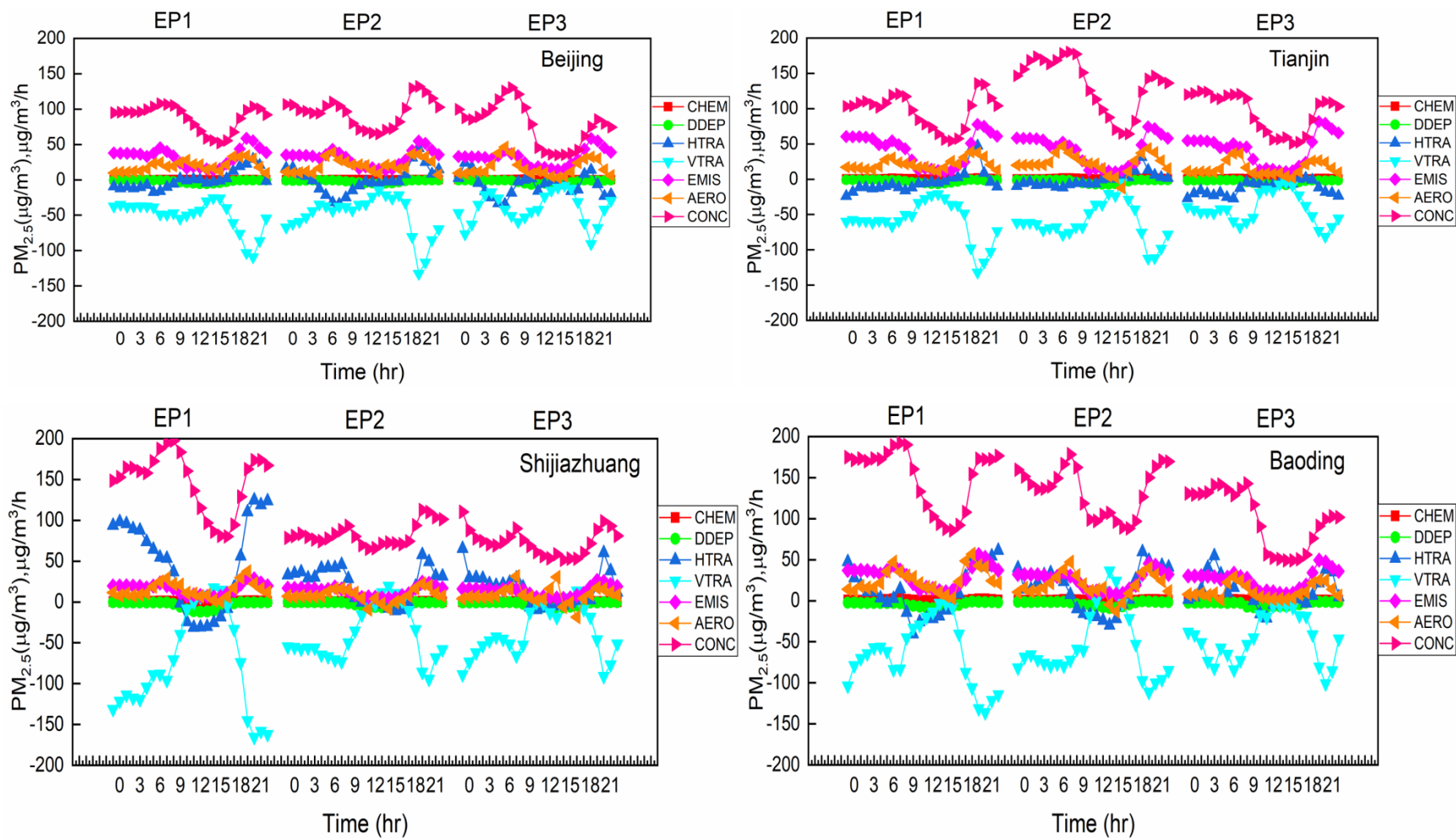
563   influenced by VTRA during the EPs.

564   Furthermore, the diel variations of the contributions of various atmospheric

565   processes to the formation of $PM_{2.5}$ as well as the hourly variations of $PM_{2.5}$ concentrations

566   at the surface layer during the three episodes are illustrated in Fig. 8. In Beijing, EMIS and

567   AERO processes were the major $PM_{2.5}$ sources, and showed two peaks (07:00 LT and

568   20:00 LT) during the three episodes.

569

570

571

Fig. 6. Hourly PM$_{2.5}$ change rates (Case 2) due to individual atmospheric processes for layers 1-10 (a-c) and evolution of hourly PM$_{2.5}$ vertical profiles (d-f) during the three pollution episodes in Tianjin. Abbreviations used in this figure are the same as in Fig. 1.

Fig. 7. Positive and negative contribution ratios of the individual processes to PM$_{2.5}$ concentrations (Case 2) at the surface layer in (a) Beijing, (b) Tianjin, (c) Shijiazhuang, and (d) Baoding during the three pollution episodes. Abbreviations used in this figure are the same as in Fig. 2.

580

Fig. 8. Diel variations of contributions of individual processes to PM$_{2.5}$ formation (Case 2) at the surface layer during the three pollution episodes in the four representative cities. Abbreviations used in this figure are the same as in Fig. 1.

581
582

31

583   The highest rates of EMIS during the EPs ranged between 54.8-58.6 μg/m^3/h, all occurred

584   at 20:00 LT. The VTRA dominated the PM$_{2.5}$ removal, with the highest removal rates of -

585   109.3 μg/m^3/h (at 21:00 LT), -132.6 μg/m^3/h (at 20:00 LT), and -90.7 μg/m^3/h (at 20:00

586   LT) during EP1, EP2, and EP3, respectively. In addition, HTRA was another major PM$_{2.5}$

587   removal pathway during the EPs. However, HTRA later acted as another PM$_{2.5}$ source

588   during EP1 (17:00-22:00 LT; with maximum rate of 29.6 μg/m^3/h at 21:00 LT), EP2

589   (00:00-03:00 and 18:00-23:00 LT; with maximum rate of 44.7 μg/m^3/h at 20:00 LT), and

590   EP3 (00:00-02:00 and 19:00-20:00 LT; with highest rate of 24.0 μg/m^3/h at 01:00 LT),

591   leading to the horizontal import of PM$_{2.5}$ during the periods. Considering Tianjin, EMIS

592   process was the dominant PM$_{2.5}$ source and exhibited two distinct peaks (00:00 LT and

593   20:00 LT) during the three episodes. The highest contributions of EMIS during EP1, EP2,

594   and EP3 were 77.7 μg/m^3/h, 74.1 μg/m^3/h, and 81.7 μg/m^3/h, respectively, all occurred at

595   20:00 LT. AERO process was another PM$_{2.5}$ source with two peaks during EP1 (07:00 LT

596   and 19:00 LT), EP2 and EP3 (07:00 LT and 20:00 LT). The negative contributions of

597   VTRA made it the dominant PM$_{2.5}$ sink throughout the 24hrs period, with the maximum

598   removal rates of -132.1 μg/m^3/h (at 20:00 LT), -112.5 μg/m^3/h (at 20:00 LT), and -81.3

599   μg/m^3/h (at 21:00 LT) during EP1, EP2, and EP3, respectively. Besides VTRA, HTRA

600   served as the second major PM$_{2.5}$ sink during the three EPs. However, HTRA later became

601   another PM$_{2.5}$ source during EP1 (16:00-21:00 LT; with maximum rate of 47.5 μg/m^3/h),

602   EP2 (14:00-23:00; with maximum rate of 31.1 μg/m^3/h), and EP3 (17:00-18:00 LT; with

603   very low rates). In Shijiazhuang, HTRA was the major PM$_{2.5}$ contributor, and showed two

604   peaks during EP1 (98.3 μg/m^3/h at 01:00 LT and 124.8 μg/m^3/h at 21:00 LT), EP2 (45.8

605   μg/m^3/h at 08:00 LT and 57.8 μg/m^3/h at 20:00 LT), and EP3 (65.2 μg/m^3/h at 00:00 LT

606   and 60.3 $\mu g/m^3$/h at 21:00 LT). The VTRA was the dominant $PM_{2.5}$ removal pathway, with

607   the highest rates of -165.6 $\mu g/m^3$/h, -94.5 $\mu g/m^3$/h, and -91.0 $\mu g/m^3$/h during EP1, EP2, and

608   EP3, respectively, all at 21:00 LT. However, VTRA later became positive and served as

609   another $PM_{2.5}$ source during EP1 (13:00-16:00 LT; with maximum rate of 17.4 $\mu g/m^3$/h at

610   15:00 LT), EP2 (14:00-17:00 with maximum rate of 19.4 $\mu g/m^3$/h at 15:00 LT), and EP3

611   (15:00-17:00 with highest rate of 13.6 $\mu g/m^3$/h at 17:00 LT), resulting to the vertical import

612   of $PM_{2.5}$ during the periods. In Baoding, EMIS, AERO, and HTRA were the major $PM_{2.5}$

613   formation pathways during nighttime, while EMIS and AERO were the dominant sources

614   during daytime. Being the major $PM_{2.5}$ removal pathway, VTRA had the highest rates of -

615   136.3 $\mu g/m^3$/h (21:00 LT), -111.4 $\mu g/m^3$/h (20:00 LT), and -101.1 $\mu g/m^3$/h (21:00 LT)

616   during EP1, EP2, and EP3, respectively. During EP2, VTRA shortly behaved as another

617    $PM_{2.5}$ source (13:00-15:00 LT, with highest rate of 36.5 $\mu g/m^3$/h. With very low rates

618   during the episodes, DDEP and CHEM processes served as $PM_{2.5}$ sink and source,

619   respectively across the four cities. The $PM_{2.5}$ concentrations peaked in Beijing (EP1: 107.8

620    $\mu g/m^3$ at 07:00 LT; EP2: 132.1 $\mu g/m^3$ at 20:00 LT; EP3: 130.3 $\mu g/m^3$ at 08:00 LT), Tianjin

621   (EP1: 135.7 $\mu g/m^3$ at 20:00 LT; EP2: 180.1 $\mu g/m^3$ at 08:00 LT; EP3: 124.6 $\mu g/m^3$ at 02:00

622   LT), Shijiazhuang (EP1: 197.6 $\mu g/m^3$ at 09:00 LT; EP2: 112.6 $\mu g/m^3$ at 20:00 LT; EP3:

623   110.3 $\mu g/m^3$ at 00:00 LT), and Baoding (EP1: 192.0 $\mu g/m^3$ at 08:00 LT; EP2: 178.2 $\mu g/m^3$

624   at 08:00 LT; EP3: 142.8 $\mu g/m^3$ at 09:00 LT).

625   **4.   Conclusions**

626   This study employed the PA tool in the CMAQ model to identify and quantify the

627   contributions of individual atmospheric processes and meteorology to the three $PM_{2.5}$

628   pollution episodes that occurred during the COVID-19 lockdown in the BTH region even

33

629   with the required reductions in human activities. Due to emission reductions, the total $PM_{2.5}$

630   concentrations across the BTH decreased by 6.2-11.0%. However, the region still

631   experienced three $PM_{2.5}$ pollution episodes during the lockdown. The IPR results showed

632   that the EMIS and AERO processes were the dominant positive contributors to the net

633   surface $PM_{2.5}$ in Beijing and Tianjin, while the EMIS, HTRA, and AERO pathways

634   dominated the net surface $PM_{2.5}$ formation in Shijiazhuang and Baoding. In Case 2, the

635   decrease in surface $PM_{2.5}$ concentrations across the BTH was primarily attributed to the

636   reduced EMIS and AERO processes, which shows the reduction in the primary source of

637     $PM_{2.5}$ as well as decrease in the formation of secondary aerosol through gas-to-particle

638   conversion. Both vertical and horizontal transport had significant impacts on the changes

639   in surface $PM_{2.5}$. Elevated $PM_{2.5}$ concentrations (in Case 2) in the BTH region during the

640   lockdown could be attributed to a low vertical transport rate of $PM_{2.5}$ from the surface layer

641   to the upper layers. Furthermore, during the three pollution episodes, EMIS and AERO

642   processes were the dominant sources of $PM_{2.5}$ formation in Beijing, Tianjin, and Baoding,

643   while HTRA was the major source in Shijiazhuang. In all of the four cities, vertical

644   transport served as the major $PM_{2.5}$ sink throughout the episodes, with differences in

645   vertical rates between the episodes in each city. The pollution levels in the four cities were

646   greatly and positively influenced by the PBLH, as the episode with the lowest PBLH had

647   the highest $PM_{2.5}$ concentration in a city. This study reveals the various atmospheric

648   processes and meteorological factors governing the $PM_{2.5}$ formation during the severe

649   pollution episodes in the BTH region, as well as the changes in the individual atmospheric

650   processes and $PM_{2.5}$ concentrations due to the lockdown measures, and shows that the

651   existing emissions control strategies could not prevent pollution episodes in the region,

652   especially during the winter period. Since it is not possible to control the aerosol and

653   transport processes, only further changes in emissions will reduce the severity of the

654   episodes. Thus, better forecasting of the conditions that would foment such episodes

655   combined with more effective emissions control strategies are urgently required to be able

656   to mitigate such future severe pollution episodes in the BTH region.

657

660

661   **Conflict of Interest**

662   The authors declare that they have no conflict of interest.

663

664   **Open Research**

665   The simulated and the observation data ($PM_{2.5}$ and meteorological variables) used in this

666   study for model evaluation and postprocessing (Figures and Tables) can be found in

667   Sulaymon et al. (2023).

668

669   **References**

670   Ambient air pollution (2021). Retrieved 28 October 2021, from
671   https://www.who.int/airpollution/ambient/health-impacts/en
672   Bashir, M. F., MA, B. J., Bilal, Komal, B., Bashir, M. A., Farooq, T. H., Iqbal, N., & Bashir,
673   M. (2020). Correlation between environmental pollution indicators and COVID-19
674   pandemic: A brief study in Californian context. Environmental Research, 187.
675   https://doi.org/10.1016/j.envres.2020.109652
676   Bhati, S., & Mohan, M. (2018). WRF-urban canopy model evaluation for the assessment
677   of heat island and thermal comfort over an urban airshed in India under
678   varying land use/land cover conditions. Geoscience Letters, 5(1).
679   https://doi.org/10.1186/s40562-018-0126-7

Boylan, J. W., & Russel, A. G. (2006). PM and light extinction model performance metrics, goals, and criteria for three-dimensional air quality models. Atmospheric Environment, 40, 4946-4959. https://doi.org/10.1016/j.atmosenv.2005.09.087

Chang, X., Wang, S., Zhao, B., Cai, S., & Hao, J. (2018). Assessment of inter-city transport of particulate matter in the Beijing-Tianjin-Hebei region. Atmospheric Chemistry and Physics, 18(7), 4843-4858. https://doi.org/10.5194/acp-18-4843-2018

Chang, X., Wang, S., Zhao, B., Xing, J., Liu, X., Wei, L., Song, Y., Wu, W., Cai, S., Zheng, H., Ding, D., & Zheng, M. (2019). Contributions of inter-city and regional transport to $PM_{2.5}$ concentrations in the Beijing-Tianjin-Hebei region and its implications on regional joint air pollution control. Science of the Total Environment, 660, 1191-1200. https://doi.org/10.1016/j.scitotenv.2018.12.474

Chauhan A., & Singh, R.P. (2020). Decline in $PM_{2.5}$ concentrations over major cities around the world associated with COVID-19. Environ. Res. 187, 109634. 10.1016/j.envres.2020.109634

Chauhan, A.K., & Singh, R.P. (2021). Effect of lockdown on HCHO and trace gases over India during March 2020. AAQR, Volume 21, Issue 4, Article Number 200445. 10.4209/aaqr.2020.07.0445.

Chen, D., Xia, L., Guo, X., Lang, J., Zhou, Y., Wei, L., & Fu, X. (2021). Impact of inter-annual meteorological variation from 2001 to 2015 on the contribution of regional transport to PM2.5 in Beijing, China. Atmospheric Environment, 260. https://doi.org/10.1016/j.atmosenv.2021.118545

Chen, L., Shi, M., Gao, S., Li, S., Mao, J., Zhang, H., Sun, Y., Bai, Z., & Wang, Z. (2017). Assessment of population exposure to $PM_{2.5}$ for mortality in China and its public health benefit based on BenMAP. Environmental Pollution, 221, 311-317. https://doi.org/10.1016/j.envpol.2016.11.080

Croft, D. P., Zhang, W., Lin, S., Thurston, S. W., Hopke, P. K., Masiol, M., Squizzato, S., van Wijngaarden, E., Utell, M. J., & Rich, D. Q. (2019). The association between respiratory infection and air pollution in the setting of air quality policy and economic change. Annals of the American Thoracic Society, 16(3), 321-330. https://doi.org/10.1513/AnnalsATS.201810-691OC

Cui, Y., Ji, D., Maenhaut, W., Gao, W., Zhang, R., & Wang, Y. (2020). Levels and sources of hourly PM2.5-related elements during the control period of the COVID-19 pandemic at a rural site between Beijing and Tianjin. Science of the Total Environment, 744. https://doi.org/10.1016/j.scitotenv.2020.140840

Dai, Q., Ding, J., Hou, L., Li, L., Cai, Z., Liu, B., Song, C., Bi, X., Wu, J., Zhang, Y., Feng, Y., & Hopke, P. K. (2021). Haze episodes before and during the COVID-19 shutdown in Tianjin, China: Contribution of fireworks and residential burning. Environmental Pollution, 286.
https://doi.org/10.1016/j.envpol.2021.117252

Dai, Q., Ding, J., Song, C., Liu, B., Bi, X., Wu, J., Zhang, Y., Feng, Y., & Hopke, P. K. (2021). Changes in source contributions to particle number concentrations after the COVID-19 outbreak: Insights from a dispersion normalized PMF. Science of the Total Environment, 759.
https://doi.org/10.1016/j.scitotenv.2020.143548

Dai, Q., Liu, B., Bi, X., Wu, J., Liang, D., Zhang, Y., Feng, Y., & Hopke, P. K. (2020). Dispersion normalized PMF provides insights into the significant changes in source

contributions to PM$_{2.5}$ after the CoviD-19 outbreak. Environmental Science and Technology, 54(16), 9917-9927. https://doi.org/10.1021/acs.est.0c02776

Emery, C., Tai, E., & Yarwood, G. (2001). Enhanced Meteorological Modeling and Performance Evaluation for Two Texas Ozone Episodes, Prepared for the Texas Natural Resource Conservation Commission. Environ International Corporation, Novato, CA.

Fan, Q., Lan, J., Liu, Y., Wang, X., Chan, P., Hong, Y., Feng, Y., Liu, Y., Zeng, Y., & Liang, G. (2015). Process analysis of regional aerosol pollution during spring in the Pearl River Delta region, China. Atmos. Environ. 122, 829-838.

Fan, H., Zhao, C., & Yang, Y. (2020). A comprehensive analysis of the spatio-temporal variation of urban air pollution in China during 2014-2018. Atmospheric Environment, 220. https://doi.org/10.1016/j.atmosenv.2019.117066

Fu, X.,Wang, T., Gao, J., Wang, P., Liu, Y., Wang, S., Zhao, B., & Xue, L. (2020). Persistent heavy winter nitrate pollution by increased photochemical oxidants in Northern China. Environ. Sci. Technol., 54, 3881-3889.

Gao, C., Li, S., Liu, M., Zhang, F., Achal, V., Tu, Y., Zhang, S., & Cai, C. (2021). Impact of the COVID-19 pandemic on air pollution in Chinese megacities from the perspective of traffic volume and meteorological factors. Science of the Total Environment, 773. https://doi.org/10.1016/j.scitotenv.2021.145545

Hopke, P. K., Croft, D., Zhang, W., Lin, S., Masiol, M., Squizzato, S., Thurston, S. W., van Wijngaarden, E., Utell, M. J., & Rich, D. Q. (2019). Changes in the acute response of respiratory diseases to PM 2.5 in New York State from 2005 to 2016. Science of the Total Environment, 677, 328-339. https://doi.org/10.1016/j.scitotenv.2019.04.357

Hu, J., Chen, J., Ying, Q., & Zhang, H. (2016). One-year simulation of ozone and particulate matter in China using WRF/CMAQ modeling system. Atmospheric Chemistry and Physics, 16(16), 10333-10350. https://doi.org/10.5194/acp- 16-10333-2016

Hu, J., Wu, L., Zheng, B., Zhang, Q., He, K., Chang, Q., Li, X., Yang, F., Ying, Q., & Zhang, H. (2015). Source contributions and regional transport of primary particulate matter in China. Environmental Pollution, 207, 31-42. https://doi.org/10.1016/j.envpol.2015.08.037

Hua, J., Zhang, Y., de Foy, B., Shang, J., Schauer, J. J., Mei, X., Sulaymon, I. D., & Han, T. (2021). Quantitative estimation of meteorological impacts and the COVID-19 lockdown reductions on NO2 and PM2.5 over the Beijing area using Generalized Additive Models (GAM). Journal of Environmental Management, 291. https://doi.org/10.1016/j.jenvman.2021.112676

Huang, J.P., Fung, J.C.H., Lau, A.K.H., & Qin, Y. (2005). Numerical Simulation and Process Analysis of Typhoon-Related Ozone Episodes in Hong Kong, p. 110.

Jiang, Y., Xing, J., Wang, S., Chang, X., Liu, S., Shi, A., Liu, B., & Sahu, S. K. (2021). Understand the local and regional contributions on air pollution from the view of human health impacts. Frontiers of Environmental Science and Engineering, 15(5). https://doi.org/10.1007/s11783-020-1382-2

Kwok, R. H. F., Napelenok, S. L., & Baker, K. R. (2013). Implementation and evaluation of PM$_{2.5}$ source contribution analysis in a photochemical model. Atmospheric Environment, 80, 398-407. https://doi.org/10.1016/j.atmosenv.2013.08.017

772 Li, L., Chen, C.H., Huang, C., Huang, H.Y., Zhang, G.F., Wang, Y.J., Wang, H.L., Lou,
773   S.R., Qiao, L.P., Zhou, M., Chen, M.H., Chen, Y.R., Streets, D.G., Fu, J.S., & Jang,
774   C.J. (2012). Process analysis of regional ozone formation over the Yangtze River
775   Delta, China using the Community Multi-scale Air Quality modeling system.
776   Atmos. Chem. Phys. 12, 10971-10987.
777 Li, L., Li, Q., Huang, L., Wang, Q., Zhu, A., Xu, J., Liu, Z., Li, H., Shi, L., Li, R., Azari,
778   M., Wang, Y., Zhang, X., Liu, Z., Zhu, Y., Zhang, K., Xue, S., Ooi, M. C. G.,
779   Zhang, D., & Chan, A. (2020). Air quality changes during the COVID-19 lockdown
780   over the Yangtze River Delta Region: An insight into the impact of human
781   activity pattern changes on air pollution variation. Science of the Total
782   Environment, 732. https://doi.org/10.1016/j.scitotenv.2020.139282
783 Li, M., Song, Y., Huang, X., Li, J., Mao, Y., Zhu, T., Cai, X., & Liu, B. (2014). Improving
784   mesoscale modeling using satellite-derived land surface parameters in the Pearl
785   River Delta region, China. Journal of Geophysical Research, 119(11), 6325-6346.
786   https://doi.org/10.1002/2014JD021871
787 Li, M., Zhang, Z., Yao, Q., Wang, T., Xie, M., Li, S., Zhuang, B., & Han, Y. (2021).
788   Nonlinear responses of particulate nitrate to NOx emission controls in the
789   megalopolises of China. Atmospheric Chemistry and Physics, 21(19), 15135-
790   15152. https://doi.org/10.5194/acp-21-15135-2021
791 Li, X., Huang, L., Li, J., Shi, Z., Wang, Y., Zhang, H., Ying, Q., Yu, X., Liao, H., & Hu,
792   J. (2019). Source contributions to poor atmospheric visibility in China.
793   Resources, Conservation & Recycling, 143: 167-177.
794 Liu, J., Mauzerall, D. L., Chen, Q., Zhang, Q., Song, Y., Peng, W., Klimont, Z., Qiu, X.
795   H., Zhang, S. Q., Hu, M., Lin, W. L., Smith, K. R., & Zhu, T. (2016) Air
796   pollutant emissions from Chinese households: A major and underappreciated
797   ambient pollution source. P. Natl. Acad. Sci. USA, 113, 7756-7761.
798 Liu, P., & Zhang, Y. (2011). Use of a process analysis tool for diagnostic study on fine
799   particulate matter predictions in the U.S. Part II: analyses and sensitivity
800   simulations. Atmos. Poll. Res. 2, 61-71.
801 Liu, T., Wang, X., Hu, J., Wang, Q., An, J., Gong, K., Sun, J., Li, L., Qin, M., Li, J., Tian,
802   J., Huang, Y., Liao, H., Zhou, M., Hu, Q., Yan, R., Wang, H., & Huang, C. (2020).
803   Driving Forces of Changes in Air Quality during the COVID-19 Lockdown Period
804   in the Yangtze River Delta Region, China. Environmental Science and Technology
805   Letters, 7(11), 779-786. https://doi.org/10.1021/acs.estlett.0c00511
806 Liu, X.H., Zhang, Y., Xing, J., Zhang, Q., Wang, K., Streets, D.G., Jang, C., Wang,
807   W.X., & Hao, J.M. (2010). Understanding of regional air pollution over China
808   using CMAQ. Part II: process analysis and sensitivity of ozone and particulate
809   matter to precursor emissions. Atmos. Environ. 44, 3719-3727.
810 Ma, J., Shen, J., Wang, P., Zhu, S., Wang, Y., Wang, P., Wang, G., Chen, J., & Zhang, H.
811   (2021). Modeled changes in source contributions of particulate matter during the
812   COVID-19 pandemic in the Yangtze River Delta, China. Atmospheric Chemistry
813   and Physics, 21(9), 7343-7355. https://doi.org/10.5194/acp-21-7343-2021
814 Mishra, R., Mishra, N.C., Singh, R., & Mishra, R. (2021). Improvement of atmospheric
815   pollution in the capital cities of US during COVID-19,
816   https://doi.org/10.1002/essoar.10505250.2

Muhammad, S., Long, X., & Salman, M. (2020). COVID-19 pandemic and environmental pollution: A blessing in disguise? Science of the Total Environment, 728. https://doi.org/10.1016/j.scitotenv.2020.138820

Orak, N. H., & Ozdemir, O. (2021). The impacts of COVID-19 lockdown on PM_{10} and SO_2 concentrations and association with human mobility across Turkey. Environmental Research, 197. https://doi.org/10.1016/j.envres.2021.111018.

Qiao, X., Tang, Y., Hu, J., Zhang, S., Li, J., Kota, S. H., Wu, L., Gao, H., Zhang, H., & Ying, Q. (2015). Modeling dry and wet deposition of sulfate, nitrate, and ammonium ions in Jiuzhaigou National Nature Reserve, China using a source-oriented CMAQ model: Part I. Base case model results. Science of the Total Environment, 532, 831-839. https://doi.org/10.1016/j.scitotenv.2015.05.108

Querol, X., Massagué, J., Alastuey, A., Moreno, T., Gangoiti, G., Mantilla, E., Duéguez, J. J., Escudero, M., Monfort, E., Pérez García-Pando, C., Petetin, H., Jorba, O., Vázquez, V., de la Rosa, J., Campos, A., Muñóz, M., Monge, S., Hervás, M., Javato, R., & Cornide, M. J. (2021). Lessons from the COVID-19 air pollution decrease in Spain: Now what? Science of the Total Environment, 779. https://doi.org/10.1016/j.scitotenv.2021.146380

Shang, X., Zhang, K., Meng, F., Wang, S., Lee, M., Suh, I., Kim, D., Jeon, K., Park, H., Wang, X., & Zhao, Y. (2018). Characteristics and source apportionment of fine haze aerosol in Beijing during the winter of 2013. Atmospheric Chemistry and Physics, 18(4), 2573-2584. https://doi.org/10.5194/acp-18-2573-2018

Sharma, S., Zhang, M., Anshika, Gao, J., Zhang, H., & Kota, S. H. (2020). Effect of restricted emissions during COVID-19 on air quality in India. Science of the Total Environment, 728. https://doi.org/10.1016/j.scitotenv.2020.138878

Shen, J., Zhao, Q., Cheng, Z., Huo, J., Zhu, W., Zhang, Y., Duan, Y., Wang, X., Antony Chen, L. W., & Fu, Q. (2020). Evolution of source contributions during heavy fine particulate matter (PM2.5) pollution episodes in eastern China through online measurements. Atmospheric Environment, 232. https://doi.org/10.1016/j.atmosenv.2020.117569

Shen, L., Wang, H., Zhu, B., Zhao, T., Liu, A., Lu, W., Kang, H., & Wang, Y. (2021). Impact of urbanization on air quality in the Yangtze River Delta during the COVID-19 lockdown in China. Journal of Cleaner Production, 296. https://doi.org/10.1016/j.jclepro.2021.126561

Shen, L., Zhao, T., Wang, H., Liu, J., Bai, Y., Kong, S., Zheng, H., Zhu, Y., & Shu, Z. (2021). Importance of meteorology in air pollution events during the city lockdown for COVID-19 in Hubei Province, Central China. Science of the Total Environment, 754. https://doi.org/10.1016/j.scitotenv.2020.142227

Shi, Z., Huang, L., Li, J., Ying, Q., Zhang, H., & Hu, J. (2020). Sensitivity analysis of the surface ozone and fine particulate matter to meteorological parameters in China. Atmospheric Chemistry and Physics, 20(21), 13455-13466. https://doi.org/10.5194/acp-20-13455-2020

Shi, Z., Li, J., Huang, L., Wang, P., Wu, L., Ying, Q., Zhang, H., Lu, L., Liu, X., Liao, H., & Hu, J. (2017). Source apportionment of fine particulate matter in China in 2013 using a source-oriented chemical transport model. Science of the Total Environment, 1476-1487. https://doi.org/10.1016/j.scitotenv.2017.06.019

862   Singh, R.P., & Chauhan, A.K. (2020). Impact of lockdown on air quality in India during
863   COVID-19 pandemic. Air Quality, Atmosphere and Health, Volume: 13, Issue: 8,
864   921-928.
865   Srivastava, A. (2021). COVID-19 and air pollution and meteorology-an intricate
866   relationship: A review. In Chemosphere (Vol. 263). Elsevier Ltd.
867   https://doi.org/10.1016/j.chemosphere.2020.128297
868   Sulaymon, I. D., Mei, X., Yang, S., Chen, S., Zhang, Y., Hopke, P. K., Schauer, J. J., &
869   Zhang, Y. (2020). $PM_{2.5}$ in Abuja, Nigeria: Chemical characterization,   source
870   apportionment, temporal variations, transport pathways and the health risks
871   assessment.   Atmospheric   Research,   237.
872   https://doi.org/10.1016/j.atmosres.2019.104833
873   Sulaymon, I. D., Zhang, Y., Hopke, P. K., Hu, J., Zhang, Y., Li, L., Mei, X., Gong, K., Shi,
874   Z., Zhao, B., & Zhao, F. (2021a). Persistent high PM2.5 pollution driven by
875   unfavorable meteorological conditions during the COVID-19 lockdown period in
876   the Beijing-Tianjin-Hebei region, China. Environmental Research, 198.
877   https://doi.org/10.1016/j.envres.2021.111186
878   Sulaymon, I. D., Zhang, Y., Hu, J., Hopke, P. K., Zhang, Y., Zhao, B., Xing, J., Li, L., &
879   Mei, X. (2021b). Evaluation of regional transport of PM2.5 during severe
880   atmospheric pollution episodes in the western Yangtze River Delta, China.
881   Journal   of   Environmental Management, 293.
882   https://doi.org/10.1016/j.jenvman.2021.112827
883   Sulaymon, I. D., Zhang, Y., Hopke, P. K., Zhang, Y., Hua, J., & Mei, X. (2021c). COVID-
884   19 pandemic in Wuhan: Ambient air quality and the relationships between criteria
885   air pollutants and meteorological variables before, during, and after lockdown.
886   Atmospheric Research, 250. https://doi.org/10.1016/j.atmosres.2020.105362
887   Sulaymon, I. D., Zhang, Y., Hopke, P. K., Hu, J., Rupakheti, D., Xie, X., Zhang, Y.,
888   Ajibade, F. O., Hua, J., & She, Y. (2021d). Influence of transboundary air pollution
889   and meteorology on air quality in three major cities of Anhui Province, China.
890   Journal   of   Cleaner   Production,   129641.
891   https://doi.org/10.1016/j.jclepro.2021.12964
892   Sulaymon, I.D., Zhang, Y., Hopke, P.K., Guo, S., Ye, F., Sun, J., Zhu, Y., & Hu, J. (2023).
893   Quantifying the contributions of atmospheric processes and meteorology to severe
894        $PM_{2.5}$ pollution episodes during the COVID-19 lockdown in the Beijing-Tianjin-
895   Hebei, China. [Dataset]. Zenodo. https://doi.org/10.5281/zenodo.7711747
896   Tang, L., Shang, D., Fang, X., Wu, Z., Qiu, Y., Chen, S., Li, X., Zeng, L., Guo, S., & Hu,
897   M. (2021). More significant impacts from new particle formation on haze
898   formation during COVID-19 lockdown. *Geophysical Research Letters*, *48*,
899   e2020GL091591. https://doi.org/10.1029/2020GL091591
900   Wang, B., Qiu, T., & Chen, B. (2014). Photochemical process modeling and analysis of
901   ozone generation. Chin. J. Chem. Eng. 22, 721-729.
902   Wang, N., Lyu, X. P., Deng, X. J., Guo, H., Deng, T., Li, Y., Yin, C. Q., Li, F., & Wang,
903   S. Q. (2016). Assessment of regional air quality resulting from emission   control
904   in the Pearl River Delta region, southern China. Science of the Total
905   Environment, 573, 1554-1565. https://doi.org/10.1016/j.scitotenv.2016.09.013
906   Wang, P., Chen, K., Zhu, S., Wang, P., & Zhang, H. (2020). Severe air pollution events
907   not avoided by reduced anthropogenic activities during COVID-19 outbreak.

Resources, Conservation and Recycling, 158. https://doi.org/10.1016/j.resconrec.2020.104814

Wang, P., Ying, Q., Zhang, H., Hu, J., Lin, Y., & Mao, H. (2018). Source apportionment of secondary organic aerosol in China using a regional source-oriented chemical transport model and two emission inventories. Environmental Pollution, 237, 756-766. https://doi.org/10.1016/j.envpol.2017.10.122

Wang, X., Li, L., Gong, K., Mao, J., Hu, J., Li, J., Liu, Z., Liao, H., Qiu, W., Yu, Y., Dong, H., Guo, S., Hu, M., Zeng, L., & Zhang, Y. (2021). Modelling air quality during the EXPLORE-YRD campaign - Part I. Model performance evaluation and impacts of meteorological inputs and grid resolutions. Atmospheric Environment, 246. https://doi.org/10.1016/j.atmosenv.2020.118131

Wang, X., Zhang, Y., Hu, Y., Zhou, W., Lu, K., Zhong, L., Zeng, L., Shao, M., Hu, M., & Russell, A.G. (2010). Process analysis and sensitivity study of regional ozone formation over the Pearl River Delta, China, during the PRIDE-PRD2004 campaign using the Community Multiscale Air Quality modeling system. Atmos. Chem. Phys. 10, 4423-4437.

Wu, C., Wang, H., Cai, W., He, H., Ni, A., & Peng, Z. (2021). Impact of the COVID-19 lockdown on roadside traffic related air pollution in Shanghai, China. Building and Environment, 194. https://doi.org/10.1016/j.buildenv.2021.107718

Xing, J., Zhang, Y., Wang, S.X., Liu, X.H., Cheng, S.H., & Zhang, Q. (2011). Modeling study on the air quality impacts from emission reductions and atypical meteorological conditions during the 2008 Beijing Olympics. Atmos. Environ. 45, 1786-1798.

Xing, J., Li, S., Jiang, Y., Wang, S., Ding, D., Dong, Z., Zhu, Y., & Hao, J. (2020). Quantifying the emission changes and associated air quality impacts during the COVID-19 pandemic on the North China Plain: A response modeling study. Atmospheric Chemistry and Physics, 20(22), 14347-14359. https://doi.org/10.5194/acp-20-14347-2020

Xue, T., Liu, J., Zhang, Q., Geng, G., Zheng, Y., Tong, D., Liu, Z., Guan, D., Bo, Y., Zhu, T., He, K., & Hao, J. (2019). Rapid improvement of PM2.5 pollution and associated health benefits in China during 2013-2017. Science China Earth Sciences, 62(12), 1847-1856. https://doi.org/10.1007/s11430-018-9348-2

Xu, W., Song, W., Zhang, Y., Liu, X., Zhang, L., Zhao, Y., Liu, D., Tang, A., Yang, D., Wang, D., Wen, Z., Pan, Y., Fowler, D., Collett, J. L., Willem Erisman, J., Goulding, K., Li, Y., & Zhang, F. (2017). Air quality improvement in a megacity: Implications from 2015 Beijing Parade Blue pollution control actions. Atmospheric Chemistry and Physics, 17(1), 31-46. https://doi.org/10.5194/acp-17-31-2017

Yan, D., Lei, Y., Shi, Y., Zhu, Q., Li, L., & Zhang, Z. (2018). Evolution of the spatiotemporal pattern of PM2.5 concentrations in China - A case study from the Beijing-Tianjin-Hebei region. Atmospheric Environment, 183, 225-233. https://doi.org/10.1016/j.atmosenv.2018.03.041

Ye, F., Rupakheti, D., Huang, L., T, Nishanth., MK, S.K., Li, L., KT, V., & Hu, J. (2022). Integrated process analysis retrieval of changes in ground-level ozone and fine particulate matter during the COVID-19 outbreak in the coastal city of Kannur, India. Environmental Pollution, 307. https://doi.org/10.1016/j.envpol.2022.119468

953   Yin, P., Brauer, M., Cohen, A.J., Wang, H., Li, J., Burnett, R.T., Stanaway, J.D., Causey,
954   K., Larson, S., Godwin, W., Frostad, J., Marks, A., Wang, L., Zhou, M., & Murray,
955   C.J.L. (2020). The effect of air pollution on deaths, disease burden, and life
956   expectancy across China and its provinces, 1990-2017: an analysis for the Global
957   Burden of Disease Study 2017. The Lancet Planetary Health 4, e386–e398.

958   Zhang, Y., Ma, Z., Gao, Y., & Zhang, M. (2021). Impacts of the meteorological condition
959   versus emissions reduction on the PM2.5 concentration over Beijing-Tianjin-Hebei
960   during the COVID-19 lockdown. Atmospheric and Oceanic Science Letters, 14(4).
961   https://doi.org/10.1016/j.aosl.2020.100014

962   Zhao, N., Wang, G., Li, G., Lang, J., & Zhang, H. (2020). Air pollution episodes during
963   the COVID-19 outbreak in the Beijing-Tianjin-Hebei region of China: An insight
964   into the transport pathways and source distribution. Environmental Pollution, 267.
965   https://doi.org/10.1016/j.envpol.2020.115617

966   Zhao, X., Wang, G., Wang, S., Zhao, N., Zhang, M., & Yue, W. (2021). Impacts of
967   COVID-19 on air quality in mid-eastern China: An insight into meteorology
968   and emissions. Atmospheric Environment, 266.
969   https://doi.org/10.1016/j.atmosenv.2021.118750

970   Zheng, B., Zhang, Q., Geng, G., Chen, C., Shi, Q., Cui, M., Lei, Y., & He, K. (2021).
971   Changes in China's anthropogenic emissions and air quality during the
972   COVID-19 pandemic in 2020. Earth System Science Data, 13(6), 2895-2907.
973   https://doi.org/10.5194/essd-13-2895-2021

974   Zheng, B., Zhang, Q., Geng, G., Shi, Q., Lei, Y., & He, K. (2020). Changes in China's
975   anthropogenic emissions during the COVID-19 pandemic. Earth System Science
976   Data Discussions, 1-20. https://doi.org/10.5194/essd-2020-355

977   Zhou, C., Zhou, H., Holsen, T. M., Hopke, P. K., Edgerton, E. S., & Schwab, J. J. (2019).
978   Ambient Ammonia Concentrations Across New York State. Journal of Geophysical
979   Research: Atmospheres, 124(14), 8287-8302.
980   https://doi.org/10.1029/2019JD030380

981   Zhu, N., Zhang, D., Wang, W., Li, X., Yang, B., Song, J., Zhao, X., Huang, B., Shi, W.,
982   Lu, R., Niu, P., Zhan, F., Ma, X., Wang, D., Xu, W., Wu, G., Gao, G. F., & Tan,
983   W. (2020). A Novel Coronavirus from Patients with Pneumonia in China, 2019.
984   New England Journal of Medicine, 382(8), 727-733.
985   https://doi.org/10.1056/nejmoa2001017